Adugna Legesse Woldemariam

Integration Of Heat Pumps for Enhancing Low Temperature District Heating Systems

School of Technology and Innovations
Major of Electrical Engineering
Master's Programme in Electrical and Energy Engineering

Vaasa 2026

UNIVERSITY OF VAASA			
School of	Technology and Innovations		
Author:	Adugna Legesse Woldemariam		
Title of the thesis:	Integration Of Heat Pumps for Enhancing Low Temperature District Heating Systems: Case: Vaasa DH		
Degree:	Master of Science in Technology		
Degree Programme:	Master's Programme in Electrical and Energy Engineering		
Supervisor:	Dr. Morteza Vahid Ghavidel		
Year:	2026	**Pages:**	80

ABSTRACT:

District heating (DH) is central to decarbonizing heating sector. Within the effort of decarbonizing the sector, the transition from third-generation district heating (3GDH) to fourth-generation low-temperature district heating (4GLTDH) systems must be performed and evaluated with care. While the feasibility of 4GLTDH systems has been studied in the technical literature, quantified comparative analyses of multiple waste heat sources under both temperature-driven (T-D) and price-driven (P-D) control within a unified dynamic framework remain rare. This thesis develops a modular MATLAB/Simulink simulation model of an integrated HP-thermal energy storage (TES)-LTDH system, parameterised on the Pätti sub-system in Vaasa. Thirteen scenarios based on three types of waste heat sources (wastewater (WW), data centers (DCs) in three configurations, and industrial waste heat (IWH) in two configurations) were evaluated in both T-D and P-D operating modes under 2024 Finnish day-ahead electricity prices, grid CO_2 factors, and ambient temperatures. Twelve performance indicators were tracked for each scenario, as well as performed a one-at-a-time sensitivity analysis on eight system parameters. Results show that WW, primary-side data center (DC-P), and air-cooled data center (DC-A) sources can be operated year-round. Secondary-side data centers (DC-S) and Industrial waste heat (IWH) configuration at 30-40 °C (IND-B) can only be operated during part of the year. The IWH configuration at 45-50 °C (IND-A) appears to be incompatible with the requirements of 4GLTDH systems. The binding compatibility threshold is 35 °C source temperature. P-D dispatch indicated 44-50% electricity cost reduction across operationally active sources, reaching 83% for the incompatible IND-A configuration where the HP barely runs. CO_2 emissions reduced by 22-76% relative to T-D though it introduces a supply reliability penalty of 1,643-5,102 MWh, which is the largest for high-coverage sources. Overall, transitioning from 3GDH to 4GLTDH systems alone will result in a 41% reduction in CO_2 emissions; the most balanced configuration (DC-P P-D) achieves the lowest specific emissions (4.66 gCO_2/kWh) at 75 % demand coverage. These findings can provide guidance for the selection of waste heat sources for HPs in other areas with similar climates, such as in the other Nordic countries.

KEYWORDS: District heating, low-temperature district heating, heat pump, waste heat recovery, thermal energy storage, price-driven control, Simulink, sensitivity analysis

Acknowledgments

I want to thank my supervisor, Dr. Morteza Vahid-Ghavidel, for his continuous advice, technical guidance and support throughout every stage of this thesis, from the initial conceptualization to the final writing. His patience and constructive feedback have been invaluable in shaping both the methodological approach and the final outcomes of this work.

I am also deeply grateful to Professor Xiaoshu Lü for proposing the thesis topic and providing the initial guidance that helped frame the scope and direction of the research.

My thanks go to the coordinators of the SMACCS Erasmus Mundus Joint Master's program for their continuous follow-up, academic guidance, and administrative support throughout my studies. I also thank all partner universities for the rich learning environment they provided. I would like to extend special gratitude to the University of Vaasa and its SMACCS coordinators, Professor Hannu Laaksonen and Ms. Marjukka Isaksen, for their unwavering support during my studies in Vaasa.

Finally, I would like to thank my family and friends who encouraged me to see this study through to completion. I am especially grateful to Aklilu Gebremariam and his family, who offered me unconditional family-like support, friendship, and encouragement from the very beginning of my studies to the end.

Use of Artificial Intelligence

During the preparation of this thesis, the author of this thesis used Grammarly AI-tool to improve the grammar and clarity. The author of the thesis takes full responsibility for the content of the thesis and confirms that all analysis, interpretations, and conclusions were developed by the author.

Contents

Figures

Tables

Abbreviations

3GDH	Third Generation District Heating
4GLTDH	Fourth Generation Low Temperature District Heating
5GDHC	Fifth Generation District Heating and Cooling
AI	Artificial Intelligence
AHP	Absorption Heat Pump
CAHHP	Compression-Absorption Hybrid Heat Pump
CDU	Cooling Distribution Unit
CHP	Compression Heat Pump
CO_2	Carbon Dioxide
COP	Coefficient of Performance
CRAC	Computer Room Air-Conditioning Unit
CRAH	Computer Room Air-Handling Unit
DC	Data Center
DC-A	Data Center Air-cooled configuration
DC-P	Data Center Primary-side cooling configuration
DC-S	Data Center Secondary-side cooling configuration
DCR	Demand Coverage Ratio
DH	District Heating
DHC	District Heating and Cooling
DHW	Domestic Hot Water

ENTSO	European Network of Transmission System Operators
FMI	Finnish Meteorological Institute
GHG	Greenhouse Gas
GPU	Graphics Processing Unit
HE	Heat Exchanger
HP	Heat Pump
IEA	International Energy Agency
IND-A	Industrial waste heat configuration at 45-50 °C
IND-B	Industrial waste heat configuration at 30-40 °C
IWH	Industrial Waste Heat
JRC	Joint Research Center
KPI	Key Performance Indicator
LCA	Life Cycle Assessment
LHP	Large-scale Heat Pump
LSP	Load Shifting Potential
LT	Low Temperature
LTDH	Low Temperature District Heating
MPC	Model Predictive Control
OAT	One-at-a-Time
P-D	Price-Driven (control strategy)
PTES	Pit Thermal Energy Storage
PtH	Power-to-Heat
RBC	Rule-Based Control
RDHX	Rear Door Heat Exchanger
RES	Renewable Energy Sources
SOC	State of Charge
SPF	Seasonal Performance Factor
T-D	Temperature-Driven (control strategy)
TES	Thermal Energy Storage
TUI	TES Utilization Index

ULTDH	Ultra-Low Temperature District Heating
WSTAR	University of Vaasa research data center facility
WW	Wastewater

1 Introduction

DH generates heat at a centralized location and distributes it through pipe networks to residences, businesses, and industry, offering significant potential for efficient large-scale use of low-carbon energy. Heat pumps are central to the next phase of this technology. By upgrading low temperature (LT) waste heat and operating preferentially when renewable electricity is abundant, they can deliver up to 25-30% of the energy transported by future European DH grids while supporting the transition to climate-neutral heating(David et al., 2017; Euroheat & Power, 2022).

1.1 Background

Decarbonization of heating is one of Europe's most challenging energy transitions (Pipicello et al., 2024). The European Climate Act and Green Deal commit the EU to climate neutrality by 2050 with an interim 55 % greenhouse gas (GHG) reduction target by 2030 (vs. 1990) yet heating and cooling still account for half of EU final energy consumption and depend mainly on fossil fuels(Euroheat & Power, 2025) . DH is widely recognised as one of the fastest and most cost-effective pathways to decarbonize this sector, particularly in dense Nordic urban areas where heat demand is high and existing DH infrastructure is well established (European Commission - JRC, 2025);(Lund, 2018). DH systems can integrate TES and renewable energy sources (RES) at scale and offer better supply security, lower costs, and lower emissions than individual heating devices.

The technology is now evolving from 3rd generation DH (3GDH, ~80-100°C supply) to fourth generation low-temperature district heating (4GLTDH), which operates at lower supply temperatures (50-70°C), integrates RES more easily, and couples to other energy grids (Capone et al., 2023). A central enabler is the recovery of underutilized energy flows such as surplus or waste heat from industrial processes and data centers (DCs), into DH networks (Zirne & Pakere, 2024). Studies show that integrating waste heat into DH improves the efficiency of both the heat supply and the recovery source, lowers fuel consumption and emissions, and reduces costs through primary energy savings (Cioccolanti et al., 2021). Combining HPs with waste heat further improves efficiency and

reduces emissions (Friedrich et al., 2025), making HP-waste heat integration a key research focus for Nordic LTDH transformation. This technology addresses the primary issues facing the EU by providing more supply security, reduced costs, and reduced greenhouse gas emissions when compared to conventional heating devices, which hinders the evolution toward smart cities.

1.2 Problem Statement

Although they represent an important part of the EU's decarbonization strategy, the majority of current DH systems operate at 3GDH temperature levels. This limits the technical and economic feasibility of integrating LT waste-heat sources, increases distribution losses, and reduces overall efficiency. At the same time, growing shares of variable renewable electricity create both an opportunity (cheap low-carbon electricity for HP operation) and a challenge that HP dispatch must be coordinated with electricity price signals and thermal storage to maximize both cost and carbon performance (Jaanto et al., 2023).

While 4GLTDH and HP integration concepts are well described in the literature, there is still a lack of quantified comparative analyses of multiple waste heat sources under both T-D and P-D control strategies within a dynamic annual simulation framework, particularly for the Finnish market context with its specific electricity price distribution and grid carbon characteristics. To address this gap, this thesis develops and applies a dynamic model of the Vaasa low-temperature district heating (LTDH) system and uses it to answer the following research questions.

1.3 Research Objectives and Questions

This thesis investigates the technical integration and operational performance of large-scale HPs in a Nordic LTDH system, with a focus on waste heat source compatibility, control strategy comparison, and environmental impact. The research questions and objectives are defined as follows:

RQ	Research Question	Objective
RQ1	Under what conditions are HP technically compatible with 4GLTDH supply temperatures across different waste heat source types?	Analyse the technical compatibility of HP with 4GLTDH systems across different waste heat source types and temperature levels
RQ2	How do source type and temperature level influence HP efficiency and annual heat contribution in LTDH?	Quantify how source type and temperature level influence HP efficiency and annual heat contribution in LTDH
RQ3	Which control strategy delivers the best balance of cost, reliability, and flexibility?	Evaluate and compare control strategies in terms of cost, reliability, and operational flexibility
RQ4	To what extent does HP integration reduce CO_2 emissions and electricity cost relative to the 3GDH baseline?	Assess the environmental and economic performance of HP integration relative to the existing baseline

1.4 Scope and Limitations

1.4.1 Scope of the Study

This thesis focuses on the technical integration and performance assessment of centrally installed large-scale electric HPs within a 4GLTDH network, using the Pått HP sub-system in Vaasa as the case study context. The work is scoped at the production and primary distribution level (interactions between HP, TES, waste heat sources, and the DH network are modelled), while building-level systems and individual consumer substations are excluded.

The analysis covers three waste heat source categories (WW treatment, DC cooling, and industrial process heat) across multiple HP configurations representing different source temperatures and cooling architectures. Each source category is evaluated under both T-D and P-D dispatch strategies, yielding thirteen simulation scenarios in total. The model is implemented in MATLAB/Simulink at hourly resolution over a full year, using real 2024

Finnish day-ahead electricity prices, ambient temperature records, and grid CO_2 emission factors as boundary conditions. The Påtti sub-system serves approximately 2,000 detached houses representing a 36 GWh annual heat demand within the broader Vaasa DH network, and this sub-system scale is used consistently throughout the analysis.

Performance is assessed using four main groups of indicators: thermodynamic efficiency (expressed through COP and SPF), supply reliability (represented by DCR), environmental performance (annual CO_2 emissions and avoided emissions), and economic performance (annual electricity cost). A one-at-a-time sensitivity analysis across eight model parameters provides additional insight into the robustness of the findings. The results are interpreted in the context of the research questions and compared against relevant Nordic and European benchmarks from the literature.

1.4.2 Limitations of the Study

The following limitations define the boundaries within which the results should be interpreted:

	Limitation	Implication
1	Hourly heat demand profile constructed from the national Finnish monthly pattern (Finnish Energy, 2026a) since actual hourly utility data from Påtti is unavailable	Demand profile may not capture the exact hourly variation of the Påtti consumer base
2	Industrial source parameters derived from literature values based on Vaasan Sähkö's reported 74 GWh annual recovery (no measured hourly operational data)	Source temperature and availability patterns carry engineering estimate uncertainty
3	DC source scaled to a hypothetical 200-rack configuration based on WSTAR specifications (no DC of this scale currently exists in Vaasa)	Results represent a forward-looking scenario rather than an existing deployment
4	Single-node thermodynamic model (pipe heat losses, hydraulic pressure dynamics, pump	DCR values represent best-case upper bounds; actual

	control, and building-side emission systems are excluded)	supply reliability would be lower
5	Economic analysis limited to annual electricity cost (investment costs, maintenance, tariff structures, and financing are excluded)	Findings address operational performance only; full techno-economic feasibility is not assessed
6	Environmental analysis limited to operational CO_2 emissions (full LCA covering equipment, refrigerant effects, and network construction is not performed)	Reported CO_2 reductions represent operational savings only
7	Legionella risk management is outside the scope (building-level TMV compliance and periodic thermal disinfection cycles are assumed per standard 4GLTDH practice)(Toffanin et al., 2021)	DHW safety implications of low supply temperatures are not quantified

1.5 Structure of the report

The thesis is organized into five chapters. Chapter 2 reviews the relevant literature on DH system evolution, LT waste heat sources, HP technologies, integration schemes, and control strategies, identifying the research gaps this thesis addresses. Chapter 3 describes the methodology, including the Vaasa case study, the MATLAB/Simulink model architecture, component modelling, control strategies, scenario definition, and performance indicators. Chapter 4 presents and discusses the simulation results across all thirteen scenarios, structured around the four research questions. Chapter 5 summarizes the main findings, contributions, and directions for future work.

2 Literature Review

2.1 District Heating System Generations

DH systems have evolved through five successive generations, each defined principally by their supply temperature, energy carrier, and integration capability (Figure 1).

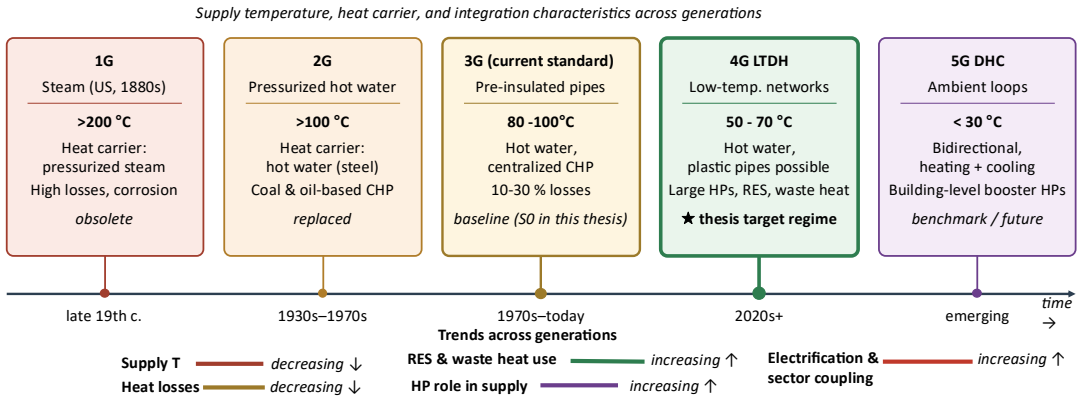

Figure 1: Evolution of DH from 1st to 5th generation(IEA DHC, 2024; Werner, 2017).

The 1st generation networks (late 19th-century US) used steam; the 2nd generation introduced pressurized hot water at supply temperatures above 100 °C; and the 3rd generation, currently the most widespread, lowered supply temperatures to between 100 °C and 80 °C to match radiator-based residential heating (IEA DHC, 2024; Werner, 2017). While 3GDH enabled centralized heat production and infrastructure reuse, it faces several limitations relevant to this thesis: distribution losses of 10-30% at high network temperatures(Danielewicz et al., 2016; Werner, 2017), reduced durability of high-temperature components (Nord et al., 2018) and incompatibility with LT renewable and waste heat sources that cannot be directly integrated at higher supply levels(Winterscheid et al., 2017).

These limitations motivated the development of 4GLTDH, characterized by supply temperatures of 50-70°C, low return temperatures, and design for integration of low-grade heat sources and large electric HPs(Lund et al., 2014). Within this category, low-temperature district heating (LTDH) operates in the 50-70°C supply range, while ultra-low temperature district heating (ULTDH) operates below 50°C and requires building-level

booster HPs for domestic hot water(D. Østergaard & Svendsen, 2017). This 4GLTDH supply range is the target condition adopted throughout this thesis, as it directly enables efficient HP operation with the waste heat sources available in Vaasa.

A fifth generation (5GDHC) has been proposed, shifting heat production to the building level using distributed booster HPs and ambient loop networks. However, 5GDHC faces significant challenges, including high distributed investment costs, stress on local electricity networks, and cost dependency on fluctuating electricity prices(Arnaudo et al., 2021; Meibodi & Loveridge, 2022; Nérot et al., 2023). For Nordic cities with existing DH infrastructure, evolution toward 4GLTDH with central large HPs is a more practical decarbonization pathway than full 5GDHC conversion, which is why this thesis focuses on 4GLTDH.

2.2 Low-temperature heat sources and waste heat

A primary motivation for adopting 4GLTDH is the opportunity to exploit LT and waste heat sources that are too low-grade for direct use in conventional DH, but well-matched to operating temperatures of 4GLTDH when upgraded by large HPs (Opadokun et al., 2025; Schmidt et al., 2017). This thesis focuses on WW, industrial, and DC waste heat as representative LT sources for the 4GLTDH system.

2.2.1 Classification of Waste Heat

Waste heat is defined as all forms of latent and sensible heat that are not the intended output of the source process (Kuta et al., 2025). The most common classification is by temperature grade: low grade (<100 °C), medium grade (100-400 °C), and high grade (>400 °C) (Mahmoud et al., 2020). High-grade waste heat from combustion processes can drive electricity generation; medium-grade exhaust streams can supply DH directly, while low-grade heat, which is the dominant fraction globally, requires upgrade through HPs to meet useful supply temperatures (Pakere et al., 2023; Z. Y. Xu et al., 2019). For LTDH, this low-grade fraction is the most relevant, since temperatures range closely match the range that compression HPs can efficiently lift to 4GLTDH supply levels.

Waste heat sources for DH are categorized into three sectors: industrial (food, metal, ceramic factories), urban (DCs, supermarkets), and utility (power plants, waste incineration) (Jodeiri et al., 2022; Mahmoud et al., 2020). Globally, the largest contributions come from industrial processes and DCs (Yuan et al., 2025). These two sectors are therefore selected for the source scenarios in this thesis, alongside the existing WW source already in operation in Vaasa.

2.2.2 Wastewater, Industrial, and Data Center Waste Heat

Wastewater treatment plants (WWTPs). WW is a widespread LT resource, with sewer temperatures typically above ambient and significantly higher and steadier flow rates at WWTP outlets than in upstream sewers (Turek et al., 2024). This makes WWTPs particularly attractive for waste heat recovery and is the rationale for selecting the Påtti facility as the WW source modelled here.

Industrial waste heat (IWH) is characterized by intermittency and load-dependency. Approximately 50% of industrial energy is rejected at low grade (30-100°C), with a major portion in the 30-40°C range (Fang et al., 2013; Turek et al., 2024). Industrial production follows its own schedule independently of heating demand, meaning that large TES and auxiliary heat sources are required alongside waste heat integration(Lund et al., 2014). IWH is therefore not a stand-alone primary heat source but a component of a wider HP-TES system. The modelling work in this thesis tests how a central HP can utilize such intermittent industrial profiles while maintaining LTDH supply reliability.

Data centers reject heat near-continuously at temperatures of 20-60°C depending on cooling architecture, making them particularly attractive for LTDH integration (Yuan et al., 2025). With the growth of AI and high-density computing, global DC waste heat generation is estimated at 70-170TWh annually, of which 35-85TWh could be effectively recovered (Yuan et al., 2025). Three cooling configurations are relevant to this thesis, which are air-cooled rear door heat exchangers (DC-A), primary-side liquid cooling (DC-P), and secondary-side liquid cooling (DC-S) since each provides different source temperatures and HP operability characteristics. They are modelled based on the WSTAR research infrastructure to evaluate how source temperature and cooling configuration influence HP

performance. Table 1 summarizes the waste heat temperature ranges by cooling system type.

Table 1. Detailed comparison of DCs' waste heat sources and their corresponding temperature levels (Pan et al., 2021; Yuan et al., 2022, 2023).

Cooling units	Cooling level	Waste heat sources	Temp. level (°C)
CRACs	Room	Return warm water	15-20
		Return hot air	25-47
CRAHs	Row	Condenser coolant	40-50
		Return hot air	25-47
HEs	Room	Return warm water	20-30
	Row	Condenser coolant	40-50
	Server	Return warm water	50-60
Two-phase refrigerant-cooling	Row	Return hot air	20-40
	Server	Condenser coolant	40-60

2.2.3 Integration Potential and Challenges

Despite clear decarbonization benefits, waste heat integration faces several practical challenges, summarized in Table 2.

Table 2: Benefits and challenges of waste heat utilization in DH systems (Opadokun et al., 2025; Vilén et al., 2024; Z. Y. Xu et al., 2019; Yuan et al., 2025).

Potential benefits	Challenges
Integration of Renewable and Waste Heat	Matching Supply and Demand (fluctuating)
Reduced Heat Loss	Complex system controls for waste heat integration
Increased Efficiency of Components	Infrastructure Costs
Lower system carbon footprint	Retrofitting Existing Buildings
Economic Advantages	distribution losses
Policy Support	Unfavourable legislation (in some regions)

The three most consequential challenges (supply-demand matching, control complexity, and infrastructure cost) are design requirements rather than barriers. This thesis directly addresses the first two by modelling HP operation jointly with thermal storage and rule-based control strategies, demonstrating how variable waste heat availability can be decoupled from fluctuating demand within a Nordic context.

A specific challenge of LTDH supply temperatures is the risk of Legionella proliferation in domestic hot water (DHW) systems, as the bacteria grow most actively between 20°C and 45 °C (Cloutman-Green et al., 2019). However, this risk is well-managed in practice through building-level measures that decouple DHW safety from network supply temperature (Toffanin et al., 2021). These building-level solutions are outside the system

boundary of this thesis. A supply temperature floor of 50°C is maintained in the model as a conservative lower bound consistent with 4GLTDH design practice.

2.3 Heat Pump Technologies in DH Systems

HPs driven by decarbonized electricity are recognized as key technologies for replacing fossil boilers in heating decarbonization. Large HPs in DH can substantially reduce emissions, although their levelized cost of heat compared to gas boilers depends on fuel and electricity prices (Javanshir et al., 2022). In LTDH, their ability to upgrade LT sources to useful supply temperatures makes them central to existing-network decarbonization. HP operates on a refrigerant cycle: heat is extracted from a source through an evaporator, compressed to a higher pressure and temperature, and rejected through a condenser at the supply temperature (Jouhara et al., 2018).

2.3.1 Performance Metrics: COP and SPF

The Coefficient of Performance (COP) is the ratio of delivered thermal energy to electrical input and is the standard hourly performance metric (Tejani, 2021). COP depends on the temperature lift between source and sink: smaller lifts yield higher COPs, while extremely cold ambient conditions or very high required supply temperatures reduce efficiency. Refrigerant choice, compressor and heat exchanger types, and operating temperatures are the primary determinants (Pieper et al., 2019; Vannoni et al., 2023).

The Seasonal Performance Factor (SPF) is the ratio of total useful thermal energy to total electrical consumption over an operating season, accounting for varying load, temperature, and usage patterns (Lorenzo & Narvarte, 2019). SPF therefore better characterizes annual system performance than instantaneous COP. This thesis applies COP at the hourly timestep within the Simulink model and reports SPF as the seasonal KPI for comparing integration concepts and control strategies.

2.3.2 HP Integration Schemes in LTDH

The placement and connection mode of the HP within the DH network strongly influence the achievable COP, network temperature levels, and the practical feasibility of using LT

heat sources (Barco-Burgos et al., 2022). Three integration archetypes are distinguished in the literature (Figure 2): centralized plant-level integration, network-level (local) integration, and decentralized building-level integration. The selection depends on existing CO_2 emissions, electricity mix, and the perspective of building owners versus network operators (Capone et al., 2023).

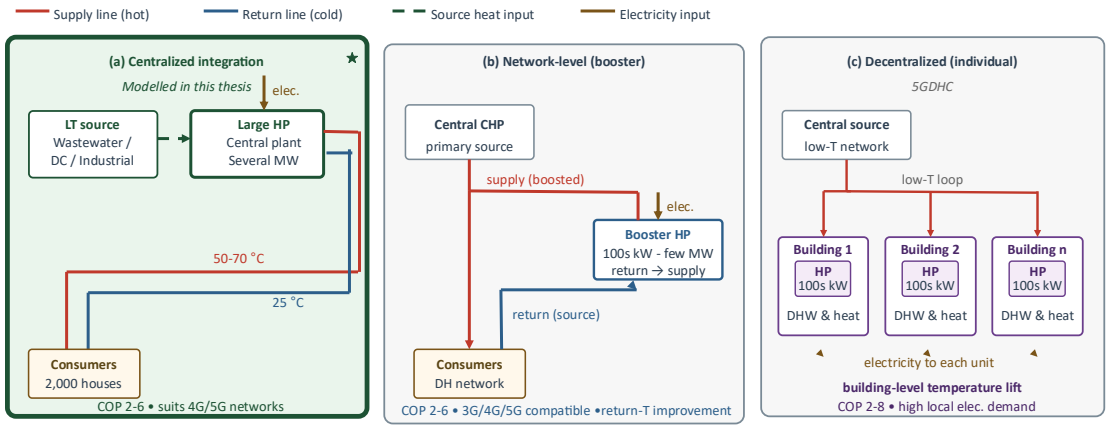

Figure 2: HP integration archetypes in DH networks.

Large-scale electric HPs installed at the central heating plant are the configuration adopted in this thesis. Central HPs extract heat from a LT source and deliver it to the DH supply network at 50-70°C, achieving COP values of 2-6 depending on source and supply temperatures (Barco-Burgos et al., 2022; Pieper et al., 2019). They can utilize multiple sources, operate in parallel or series, and integrate with seasonal thermal storage to shift operation toward low-price electricity periods (Jokinen et al., 2022). Alternative integration modes such as network-level booster HPs and decentralized building-level HPs are described in the literature (Barco-Burgos et al., 2022; Ochs et al., 2022), but are not the focus of this thesis, as they require different temperature regimes and system architectures incompatible with the Pätti configuration. They also documented a range of HP placement and connection configurations in the literature depending on temperature lift and connection modes.

2.3.3 Large-Scale HP Types and Source Compatibility

HPs are classified by driving energy as compression (CHP, electrically driven) or absorption (AHP, thermally driven). CHPs achieve COPs of 1.5-6.0 with simple structure and control (Han et al., 2021; Wu et al., 2021), upgrading sources from −22°C to deliver heat

at 40-70°C for buildings (Tan et al., 2024) or from 40-70°C to 90-140°C for industrial processes (Jiang et al., 2022). Their adaptability to very low ambient temperatures is limited (Ji et al., 2026), and lubricant thermal stability constrains discharge temperatures to below 150°C (Ma et al., 2024). AHPs use thermal energy as the driver and are classified as Type I AHPs (heat amplifiers) (Zhai & Wu, 2021) and Type II AHPs (heat transformers)(Cudok et al., 2021; Gong et al., 2025). AHP COPs remain lower than CHPs, limiting their use where high efficiency and large temperature lifts are simultaneously required (Ji et al., 2026). Compression-absorption hybrid heat pumps (CAHHP) combine the strengths of both cycles to extend the operating range (Ji et al., 2026).

Most large HPs in Nordic DH systems are electrically driven CHPs coupled to low-to-medium-temperature sources. This thesis models CHPs using performance maps representative of WW, DC, and industrial sources. Absorption and hybrid technologies are noted as relevant for future extensions involving higher-temperature ranges but lie outside the scope of this work.

2.4 Flexibility: Sector Coupling, Power-to-Heat, and Thermal Storage

2.4.1 Power-to-Heat and the Finnish Electricity Market

Power-to-Heat (PtH) represents the conversion of electricity into thermal energy via HPs, enabling sector coupling between the electricity and heating networks (Pastore, 2026). In the context of LTDH, a centrally installed large HP operated as a PtH unit can shift electricity consumption to periods of low price and high renewable generation, reducing both operating costs and grid carbon emissions simultaneously (Gjorgievski et al., 2021). This co-benefit is particularly relevant in the Finnish electricity market, where day-ahead prices on the NordPool platform are positively correlated with grid CO_2 emission intensity. High prices coincide with fossil-fuel peaking plant dispatch during cold winter periods, while low prices correspond to periods of high wind and nuclear generation. A price-responsive HP dispatch strategy therefore simultaneously reduces electricity cost and carbon emissions. The 2024 Finnish day-ahead price data used as a boundary condition

in the model reflects this market structure, with R = 0.675 correlation between hourly price and grid CO_2 factor observed in the simulation year.

2.4.2 Thermal Energy Storage

TES plays a central role in enabling HP flexibility by decoupling heat production from instantaneous demand. In DH systems, TES is used for peak shaving, load shifting, integration of renewable surplus, and cost-based HP dispatch (Christensen et al., 2024; Guelpa & Verda, 2019). For DH, the most common implementations are sensible Tank Thermal Energy Storage (TTES) for daily and weekly cycles and large Pit Thermal Energy Storage (PTES) for seasonal storage, both using water as a storage medium (J. Xu et al., 2014). The Vaskiluoto TES in Vaasa has a capacity of approximately 11GWh (Vaasan Voima, 2024) provides the large-scale storage context for this thesis since the simulation model uses a representative 470MWh sub-system TES scaled to the Pätti HP capacity.

The synergy between HPs and TES is central to the flexibility proposition of this thesis. HPs convert variable renewable electricity into stored heat, while TES decouples production from consumption. The HP can therefore operate during low-price or high-renewable hours regardless of instantaneous demand, transforming an intermittent renewable resource into a dispatchable heat supply. The Simulink model represents this synergy explicitly, with TES state-of-charge as a key state variable.

2.5 Modelling and Control Strategies

2.5.1 Modelling Approach and Simulation Tools

DH system modelling approaches range from detailed coupled hydraulic-thermal dynamic models, which capture pipe transmission delays and spatial temperature distributions, to single-node energy balance representations, which sacrifice resolution for computational efficiency and suitability for control-strategy evaluation at the system level (Dancker & Wolter, 2021; Zhang et al., 2021). Within this continuum, three categories are conventionally distinguished by their treatment of dynamics: steady-state, quasi-dynamic (steady-state hydraulics with dynamic thermal behaviour), and fully dynamic.

Hydraulic and thermal sub-problems may be solved either in a coupled formulation via the Newton-Raphson method or in a decoupled (sequential) formulation, with the node method and plug-flow method being the most widely validated thermal-discretization techniques (Kuntuarova et al., 2024).

For system-level analysis focused on energy balances, HP performance, and operational strategy comparison, single-node models with assumed steady-state hydraulics are well-established (Dibos et al., 2024; Kuntuarova et al., 2024). This thesis therefore adopts a steady-state single-node energy balance at the network level, with dynamic component models for the HP and TES and time-varying exogenous inputs (electricity price, ambient temperature, supply-temperature curve, source profiles). The model is solved at hourly resolution over 8,760 timesteps, providing the temporal granularity required to evaluate control strategies while remaining consistent with the system-level focus of the analysis.

Several simulation tools are available. Domain-specific commercial packages such as STANET, TRNSYS, and ROKA3 offer well-developed user interfaces and customer support but limited flexibility for custom control logic(ROKA3, 2026; STANET, 2026; TRNSYS, 2026). MATLAB/Simulink supports dynamic simulation of complex thermo-hydraulic systems through a modular block-based structure with straightforward integration of external signals such as electricity prices and weather data (MathWorks, 2026). It is therefore well-suited to evaluating different HP integration schemes and operational strategies in LTDH at hourly resolution over a full year, and is the framework adopted here.

2.5.2 Control Strategies

Control strategies for HP operation in DH systems fall into two broad categories: rule-based control (RBC) and model predictive control (MPC) (Wang et al., 2025). RBC uses fixed logical conditions (if (condition) then (action)) and is simple to implement and transparent to interpret (Mugnini et al., 2024; Péan et al., 2019). MPC uses a predictive model to optimize future HP operation against an objective function, offering better performance but requiring detailed system models, high-quality forecasts, and significant computational effort (Drgoňa et al., 2020). While MPC has demonstrated strong performance in research settings, its implementation complexity places it beyond the practical

scope of this thesis. This work therefore evaluates two well-designed rule-based strategies (T-D and P-D), which represent practically implementable operational approaches directly relevant to DH operators.

2.6 Research Gaps and Thesis Contribution

Although the literature demonstrates the technical feasibility of LTDH and HP integration, most studies analyse either the thermodynamic performance of HPs in isolation or the potential of individual waste heat sources. As a result, the modelling of combined system-level interaction between multiple source types, a central large-scale heat pump, thermal storage, and realistic operational constraints is still not sufficiently addressed within a unified dynamic framework. Comparative scenario analyses covering multiple waste heat sources under both T-D and P-D dispatch strategies are particularly rare for Nordic LTDH systems.

On the operational side, while PtH and sector coupling literature highlights the potential for price-responsive HP dispatch, most DH studies either assume simple load-following control or focus on advanced MPC strategies that are difficult to implement in practice. Quantified comparisons of rule-based T-D versus P-D strategies across multiple source types with explicit modelling of Finnish electricity price signals and grid CO_2 factors are not found in the reviewed literature.

This thesis addresses both gaps by developing a dynamic Simulink-based model of a Nordic LTDH system that integrates a central large-scale HP, three waste heat source categories, a TES, and two rule-based control strategies. The system is evaluated through thirteen scenarios with hourly resolution over a full year. By doing so, the study provides system-level performance assessment under realistic operational constraints directly applicable to the Vaasa DH network and comparable Nordic utilities.

3 Methodology

3.1 Methodological Framework

The methodological workflow proceeds in eight sequential steps from system definition to performance evaluation, as summarized in Figure 3. Boundary conditions (case study definition, demand profile, source characterization, and external input signals) are established first, the simulation model is then formulated component by component, control strategies and scenarios are defined, the model is executed, and the results are post-processed into the KPI set used for the comparative analysis in Chapter 4.

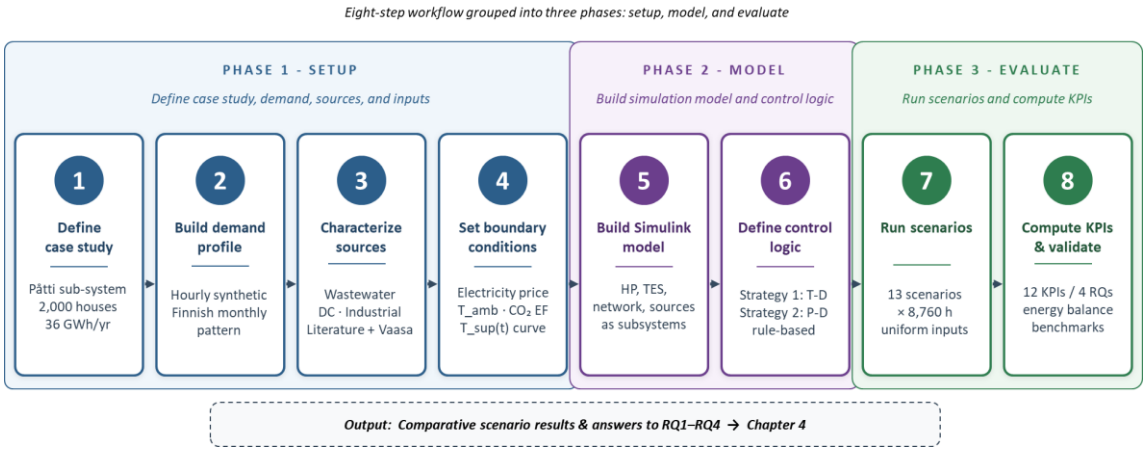

Figure 3: Methodological workflow showing the eight sequential steps of the thesis approach, from case-study definition through to KPI-based scenario comparison.

3.2 System Description and Case Study

3.2.1 System Boundaries and Reference Configurations

The system analysed is a centralized production-level LTDH system supplying heat to a Nordic urban network, like Vaasa, Finland. The system boundary extends from production to delivery of useful heat to end-users, excluding upstream fuel and electricity production as well as detailed building-level dynamics (Figure 4).

The reference system is the Pätti WW HP facility in Vaasa, which is a large-scale HP installation recovering thermal energy from treated municipal WW at source temperatures of 10-15°C and upgrading it to DH supply temperatures. The plant serves about 2,000

detached houses, contributing around 5.4% of Vaasa's total DH production of 764GWh (41 GWh annually)(Elomatic, 2024; Vaasan Sähkö, 2026).

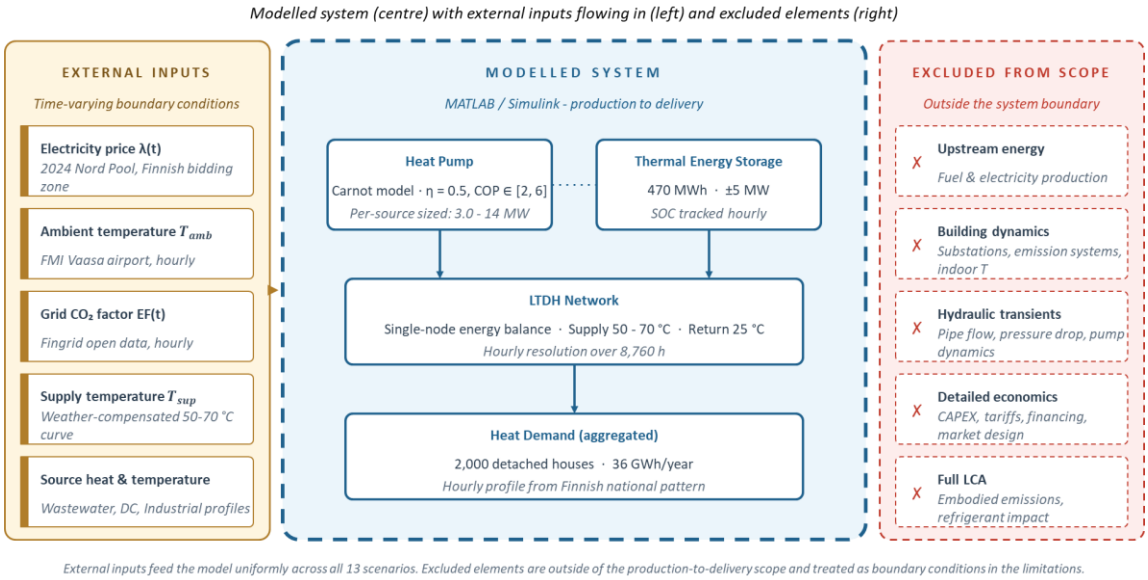

Figure 4: System boundary diagram showing included elements and excluded elements.

Two reference configurations are modelled. The first is the current 3GDH configuration, in which the HP operates at the existing Pått supply temperatures of up to 95°C(Elomatic, 2024). The second is a transformed 4GLTDH configuration, in which the same HP and consumer base operate within a modernized network at supply temperatures of 50-70°C following a weather-compensated heat curve.

3.2.2 Heat Demand Profile

The sub-network represents the space heating and domestic hot water requirements of 2,000 detached houses in the Vaasa region, with a total annual consumption of;

$$Q_{annual} = 2{,}000 \times 18\,MWh = 36\,GWh \quad (1)$$

This value is derived from Pått HP consumer base and the Finnish Energy national average detached house DH consumption of 18 MWh/year (Oulun Energia, 2023). Since hourly metered data from the Pått consumer base are not publicly available, the hourly demand profile is constructed synthetically by distributing the 36 GWh annual total according to the national Finnish monthly DH demand pattern (Finnish Energy, 2026), which exhibits a pronounced winter peak and low summer demand. Although these

statistics aggregate Finnish-wide data rather than Vaasa-specific demand, they capture the climatic seasonal variation typical of Nordic DH systems and provide a consistent reference profile across all scenarios. The full disaggregation procedure (monthly, weekly, and diurnal layers) is described with the heat demand model in section 3.3.6.

3.2.3 Waste Heat Source Overview

Three representative LT waste heat sources are evaluated. The selection is based on the literature review (section 2.2) and Vaasa's existing and emerging infrastructure (Table 3), namely WW, DC waste heat, and IWH. Detailed source models, including temperature dynamics, recoverable heat formulations, and the three DC and two industrial sub-configurations, are presented in section 3.3.5.

Table 3: Waste heat source characteristics for Vaasa context (Lu et al., 2024; Vaasan Sähkö, 2026; WSTAR, 2025).

Source	Source temp. (°C)	Recoverable heat	Availability	Vaasa relevance
WW (Påtti)	10-15	4,300-8,600 kW	Continuous, seasonal	Existing Påtti HP
DC waste heat (WSTAR)	20-45	25 kW/rack	Continuous, minor variation	Hypothetical 200-rack scale-up
IWH	30-50	up to 9,250 kW (mean)	Process-dependent, daily/weekly	74 GWh recovered in 2024

3.2.4 External Inputs and Boundary Conditions

The model uses four time-varying external signals applied uniformly across all scenarios to ensure full comparability. All signals are 8,760 hourly values for the 2024 reference year (Appendix A).

3.2.4.1 Day-ahead electricity price λ(t) [€/kWh]

Hourly NordPool spot prices for the Finnish bidding zone, drawn from the ENTSO-E Transparency Platform (Transparency Platform, 2026). Prices drive operating cost calculations and provide the dispatch signal for the P-D control strategy (section 3.4.2).

3.2.4.2 Ambient temperature T_{amb}(t) [°C]

Hourly observations for Vaasa airport from the Finnish Meteorological Institute (FMI, 2026). T_{amb}(t) drives the T-D control strategy (section 3.4.1) and the weather-compensated supply temperature curve below (section 3.2.4.4).

3.2.4.3 Grid CO_2 emission factor EF(t) [gCO_2/kWh]

Hourly Finnish grid carbon intensity from Fingrid's open data portal (Fingrid, 2026), used in post-simulation calculation of HP-related CO_2 emissions (section 3.6).

3.2.4.4 Network supply temperature T_{sup}(t) [°C]

In the 4GLTDH configuration, T_{sup}(t) is not fixed but follows a weather-compensated heat curve varying linearly with ambient temperature(Pakere et al., 2023):

$$Tsup(t) = max\big(50,\ min\big(70,\ 70 - 0.54 \cdot (Tamb(t) + 20)\big)\big)\ [°C] \qquad (2)$$

The slope of 0.54°C/°C corresponds to the supply temperature range (20°C) divided by the outdoor temperature range from the design point (−20°C) to the heating cutoff (17°C). The lower bound of 50°C reflects the minimum network temperature required to meet DHW year-round, and the upper bound of 70°C is the design supply temperature at coldest Vaasa conditions. The return temperature is held at a constant 25°C, consistent with the 4GLTDH design practice of 20-30°C (D. S. Østergaard et al., 2022); since modelling it as a time-varying signal would require building-side substation dynamics.

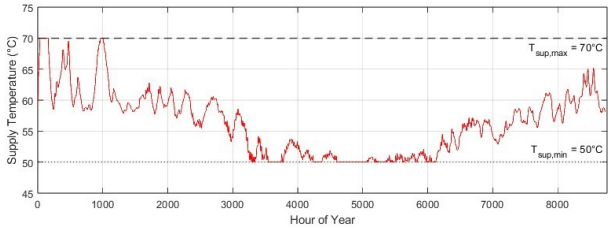

Figure 5: weather-compensated LTDH supply temperature (Vaasa, 2024).

These four signals are implemented as From Workspace blocks in Simulink and are routed to the relevant model components (HP, control strategies, post-processing) as described in section 3.3.

3.3 Simulation Model in MATLAB/Simulink

3.3.1 Overall Model Architecture

The integrated HP-LTDH system is implemented in MATLAB/Simulink R2024b as a modular hourly dynamic simulation over a full calendar year (8,760-time steps). The model

comprises HP, TES, LTDH Network, Waste Heat Source, Heat Demand, and Supply Temperature subsystems coordinated by a Control Strategy subsystem that receives external input signals and produces dispatch setpoints at each time step. Figure 6 illustrates the overall architecture and data flow between subsystems. All subsystems exchange signals through Simulink bus connections, with Unit Delay blocks on feedback paths to prevent algebraic loops. Post-processing KPI calculations are performed in MATLAB scripts applied uniformly to the Simulink output workspace after each simulation run.

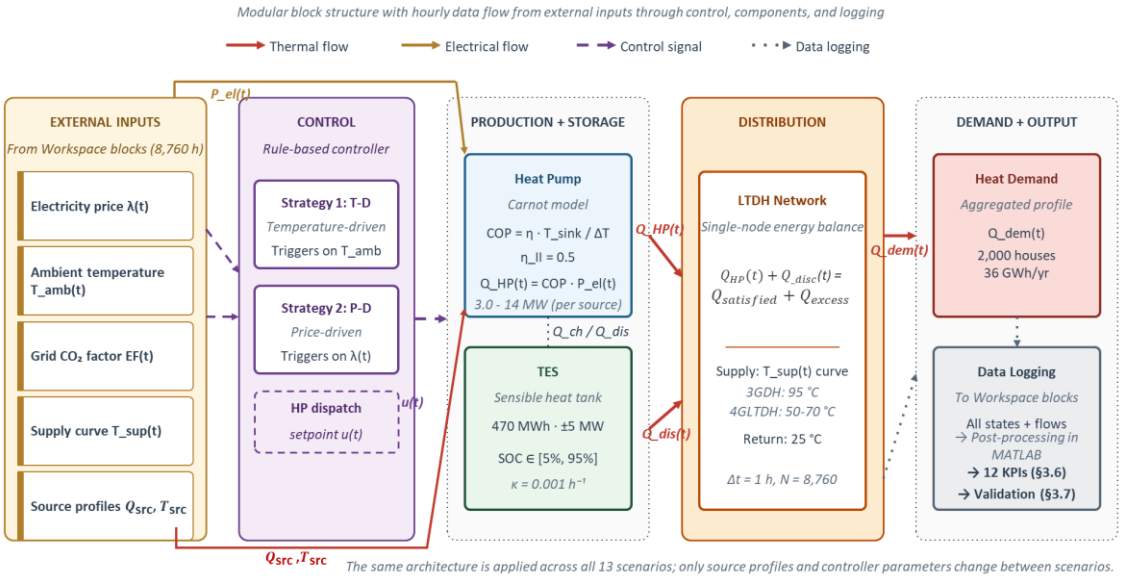

Figure 6: Simulink model architecture.

3.3.2 Heat Pump Model

The HP is modelled as a single-stage compression unit using the Carnot efficiency formulation (Pieper et al., 2019; Vannoni et al., 2023):

$$COP(t) = \eta \times \frac{T_{sup}(t)+273.15}{(T_{sup}(t)+273.15)-(T_{source}(t)+273.15)} \quad (3)$$

where temperatures are input in °C and converted to Kelvin for thermodynamic consistency. $\eta = 0.5$ is the Carnot efficiency factor representing the fraction of ideal Carnot performance achieved by a real large-scale CHP, consistent with values in the literature (Pieper et al., 2019). The computed COP is clamped to the physically feasible range [2.0, 6.0] to prevent unrealistic values at extreme temperature conditions(Barco-Burgos et al., 2022).

A minimum temperature lift gate is enforced at each time step to represent the practical operability limit of the compression cycle. For large-scale CHPs, the practical minimum operationally meaningful temperature lift is typically 10°C to 20°C (Gasser et al., 2017) while 15°C is used in this work. If the temperature difference between supply and source falls below the minimum lift threshold $\Delta T_{lift,min}$ = 15°C, the HP is forced off regardless of the control strategy signal:

$$u_{lift}(t) = \begin{cases} 1 & if\ T_{sup}(t) - T_{sour}(t) \geq \Delta T_{lift,min} \\ 0 & otherwise \end{cases} \quad (4)$$

This gate is particularly significant for industrial and data center sources during warm periods when source temperatures approach supply temperatures, and its sensitivity is explicitly examined in section 3.5.2.

The HP thermal output is determined from the available recoverable source heat using the energy balance relationship between the evaporator heat input $Q_{source}(t)$, the compressor electrical work $Q_{el,HP}(t)$, and the condenser heat output $Q_{HP}(t)$:

$$Q_{HP}(t) = Q_{source}(t) + Q_{el,HP}(t) \quad (5)$$

which, combined with the COP definition $COP(t) = \frac{Q_{HP,max}(t)}{Q_{el,HP}(t)}$ (Ivezić et al., 2023), gives:

$$Q_{HP}(t) = Q_{source}(t) \times \frac{COP(t)}{COP(t)-1} \quad (6)$$

The actual HP heat output at each time step is then constrained by the control setpoint, the nominal HP capacity, and the lift gate signal:

$$Q_{HP,actual}(t) = min\left(Q_{HP,nom}, Q_{HP,set}(t)\right).u_{lift}(t) \quad (7)$$

where $Q_{HP,nom}$ is the nominal thermal capacity of the HP, and $Q_{HP,set}(t)$ is the thermal power setpoint from the control strategy. $Q_{HP,nom}$ is sized individually to each source using the following design criterion:

$$Q_{HP,nom} = Q_{source,peak} \times \frac{COP_{design}}{(COP_{design} - 1)} \quad (8)$$

Where $Q_{source,peak}$ is the peak recoverable source heat at design conditions and $COP_{design} = 3$ is the representative mid-season 4GLTDH COP(Barco-Burgos et al., 2022). The corresponding electrical consumption is:

$$Q_{el,HP}(t) = \frac{Q_{HP,\,actual}(t)}{COP(t)} \tag{9}$$

when $COP(t) > 0$, the HP subsystem receive $Q_{source}(t)$, $Q_{HP,set}(t)$, $T_{sour}(t)$, $T_{sup}(t)$, and $Q_{HP,nom}$ as input and deliver $Q_{HP,actual}(t)$, $Q_{el,HP}(t)$, $COP(t)$, and $u_{lift}(t)$ as the outputs to the LTDH network balance, TES charging logic, and post-processing KPI blocks at each time step.

3.3.3 Thermal Energy Storage Model

The TES is a short-term buffer store sized by scaling Vaskiluoto's 11GWh capacity to the 36GWh sub-network demand, with a thermodynamic correction for the lower 4GLTDH supply temperature. Vaskiluoto's capacity is achieved at about 95°C supply (Vaasan Voima, 2024), whereas the modelled LTDH supply is capped at 70°C. Since sensible hot-water storage capacity scales with the usable temperature difference (ΔT), assuming return temperatures of 45 °C for the existing system(Finnish Energy, 2026) and 25 °C for LTDH, stored thermal energy will be;

$$E_{TES,LTDH} = E_{Vaskiluoto} \times \frac{\Delta T_{LTDH}}{\Delta T_{3GDH}} \times \frac{Q_{sub}}{Q_{Vaasa}} \tag{10}$$

where $Q_{Vaasa} = 764GWh$ (Vaasan Sähkö, 2026). The scaling yields 466MWh, rounded to 470MWh for the model.

Energy balance. The single-node model tracks stored thermal energy over $\Delta t = 1\,h$:

$$E(t + \Delta t) = E(t) + [Q_{in}(t) - Q_{out}(t) - Q_{loss}(t)]\Delta t \tag{11}$$

Where, $Q_{in}(t)$ and $Q_{out}(t)$ are the actual charging and discharging power flows, and standing losses are modelled proportionally to stored energy:

$$Q_{loss}(t) = k_{loss} \times E_{TES}(t), \qquad k_{loss} = 0.0005h^{-1} \tag{12}$$

equivalent to ≈1.2%/day, typical for insulated buffer tanks(Guelpa & Verda, 2019).

The state of charge is computed as:

$$SOC(t) = \frac{E_{TES}(t)}{E_{max}} \quad (13)$$

Constraints. Maximum charge/discharge power is scaled from Vaskiluoto's 110MW rating ($P_{max} \approx 5MW$); charging is permitted only when $SOC(t) < 0.95$, discharging only when $SOC(t) > 0.05$. The integrator initializes at $SOC_0 = 0.5$ and is bounded between 0 and 470MWh. The subsystem receives $Q_{charge,set}(t)$ and $Q_{discharge,set}(t)$as setpoints from the control strategy and delivers $Q_{charge,actual}(t)$, $Q_{discharge,actual}(t)$, $E_{TES}(t)$, and $SOC(t)$ to the LTDH network model and control logic.

3.3.4 LTDH Network model

The LTDH network is represented as a single-node energy balance at hourly resolution. Network supply temperature is determined by the weather-compensated heat curve in section 3.2.4.4 and feeds directly into the HP COP and minimum lift gate calculations.
At each time step, total available supply is:

$$Q_{total}(t) = Q_{hp,actual}(t) + Q_{discharge,actual}(t) \quad (14)$$

The instantaneous power balance $\Delta Q(t) = Q_{total}(t) - Q_{demand}(t)$ determines three mutually exclusive outputs:
When $\Delta Q(t) \geq 0$;
$Q_{satisfied}(t) = Q_{demand}(t)$, $Q_{excess}(t) = \Delta Q(t)$, $Q_{unmet}(t) = 0$

when $\Delta Q(t) < 0$;
$Q_{satisfied}(t) = Q_{total}(t)$, $Q_{excess}(t) = 0$, $Q_{unmet}(t) = |\Delta Q(t)|$

Surplus $Q_{excess}(t)$ is directed to additional TES charging subject to the SOC and P_{max} constraints of section 3.3.3. $Q_{unmet}(t)$is a slack variable representing demand that cannot be met by the HP-TES combination at timestep t. It is logged as the unmet-demand

KPI but is not explicitly back-supplied by an auxiliary boiler or any external heat source, allowing the comparative analysis to reveal HP-TES sizing constraints.

Hydraulic dynamics, pipe heat losses, and substation-level temperature variations are excluded, as the primary interest of the study lies in energy quantities such as heat production, storage utilisation, and supply shortfalls rather than short-timescale hydraulic transients. Similarly surplus heat is logged transparently as Q_{excess}in the network energy balance. DCR values therefore represent upper bounds on actual supply reliability, as noted in section 1.4.2. This is consistent with the steady-state single-node approach standard for system-level HP-LTDH studies (Dibos et al., 2024)

3.3.5 Waste Heat Source Models

All source configurations share the same model structure: a load-dependent temperature signal $T_{source}(t)$ and recoverable heat $Q_{source}(t)$, both supplied as time-varying inputs to the HP subsystem (Appendix B). Source-specific parameters are defined below.

3.3.5.1 Wastewater heat source

The WW source represents the existing Pått facility, which recovers heat from treated WW discharged from the Pått treatment plant (~6.5 million m³/year) serving Vaasa, Mustasaari, and Maalahti (Vaasan Vesi, 2024). The source temperature is modelled as the mean WW temperature with superimposed sinusoidal daily and seasonal variations:

$$T_{ww}(t) = T_{base} + \Delta T_{daily(t)} + \Delta T_{seasonal(t)} \quad (15)$$

Where T_{base} = 12.5°C is the mid-range of the 10-15°C values for the Pått facility and the two variation terms are sinusoids with 24-*h* and 8,760-*h* periods respectively, calibrated to keep $T_{ww}(t) \in [10,15]$℃ year-round.

The recoverable heat is derived from a heat-transfer balance across the HP evaporator. The mean volumetric flow rate of $\dot{V}_{ww} = \frac{6.5\times10^6}{8{,}760} = 0.206\ m^3/s$ gives $\dot{m}_{ww} = 206\ kg/s$. Cooling the WW from $T_{ww}(t)$ to a minimum permissible outlet of 5°C (lower extraction restricted by biological-treatment requirements):

$$Q_{ww}(t) = \dot{m}_{ww} \times Cp \times (T_{ww}(t) - 5) = 206 \times 4.18 \times (Tww(t) - 5) \quad (16)$$

with $C_p = 4.18\ kJ/kg \cdot °C$, yielding 6,460kW at the annual mean WW temperature of 12.5°C. A saturation block prevents $Q_{ww}(t)$from becoming negative under numerical edge conditions.

3.3.5.2 Data Center Waste Heat Source (WSTAR)

The DC waste heat source modelled in Scenarios S2a- S2f is based on the WSTAR (joint EU Next Generation EU and Academy of Finland project) research DC at the University of Vaasa (WSTAR, 2025). WSTAR comprises three rack types: Rack 1 (air-cooled with rear-door heat exchanger, RDHX), Rack 2 (direct-to-chip liquid-cooled), and Rack 3 (GPU) (WSTAR, 2025). While the physical facility operates at research scale, the rapid growth of AI computing and EU policy on edge DCs in DH substations make multi-rack deployments a plausible near-future scenario (Yuan et al., 2025). The WSTAR DC is therefore scaled to a hypothetical 200-rack deployment, retaining each rack type's cooling architecture as the basis for scaling. Three configurations represent different extraction points in the cooling system, isolating the effect of cooling architecture on HP operability and 4GLTDH compatibility (RQ1).

DC IT load is relatively stable but exhibits short-term variation from user activity, schedules, and seasonal effects(Stanica et al., 2021). The shared IT load signal is:

$$IT_{load}(t) = (L_{base} + L_{daily}(t)) \times F_{week}(t) \times F_{season}(t) \quad (17)$$

Where $L_{base} = 0.90$ (90 % continuous utilisation), $L_{daily}(t) = 0.05\, sin(^{2\pi t}/_{T_{day}})$, captures diurnal fluctuation (0.05=amplitude), $F_{week}(t)$= 0.95 (Saturday) / 0.90 (Sunday) /1.0 (weekdays), and $F_{season}(t)$applies ±3.5% sinusoidal annual modulation. The combined $IT_{load}(t)$ranges from 0.85 to 0.97.

For all three configurations, source temperature scales linearly with IT load and recoverable heat scales linearly with the per-rack thermal dissipation:

$$T_{DC,i}(t) = \mathrm{T}_{min,i} + s_i \times (IT_{load}(t) - 0.85) \quad (18)$$

$$Q_{DC,i}(t) = N_{rack} \times P_{rack} \times \alpha_i \times IT_{load}(t) \quad (19)$$

where N_{rack}= 200, $\alpha_i$is a recovery factor (1.0 except for DC-P, where the CDU_HX extraction recovers only 138/155 ≈ 0.89 of the secondary-side heat per(Lu et al., 2024)), and the configuration-specific parameters are given in Table 4. The HP nominal capacity is sized at $Q_{HP,nom,i} = Q_{DC,i,max} \times \frac{COP_{design}}{COP_{design}-1}$ as described in section 3.3.2.

Table 4: DC configuration parameters (Lu et al., 2024; Yuan et al., 2023, 2025).

Config.	Extraction point	T_{min}-T_{max} (°C)	Slope s	P_{rack} (kW)	Recovery α	$Q_{DC,max}$ (kW)	$Q_{HP,nom}$ (MW)
DC-S	Secondary-side, Rack 2 CDU after HX2	37-45	66.67	25	1.00	5,000	7.5
DC-P	Primary-side, Rack 2 CDU after CDU_HX	30-35	41.66	25	0.89	4,450	6.7
DC-A	Air-cooled, Rack 1 RDHX water loop	20-30	83.30	10	1.00	2,000	3.0

Each configuration delivers its $Q_{DC,i}(t)$and $T_{DC,i}(t)$to the HP subsystem at each hourly timestep.

3.3.5.3 Industrial Waste Heat Source

The industrial source uses Vaasan Sähkö's documented 74GWh annual waste heat recovery as the capacity basis (Vaasan Sähkö, 2026). Two temperature sub-cases are modelled, which are IND-A (45-50°C) and IND-B (30-40°C), reflects the low-grade cooling-loop fraction most suitable for HP integration in DH(Fang et al., 2013; Pakere et al., 2023). Assuming 8,000 operating hours per year typical of industrial facilities with scheduled maintenance (Gómez- de- Arteche -Botas et al., 2025), the baseline thermal power is $Q_{ind,base} = 74{,}000/8{,}000 = 9.25MW$ and the HP nominal capacity is $Q_{HP,nom} = Q_{ind,base} \times 3/2 = 14MW$.

Industrial heat availability follows process production schedules that exhibit daily and weekly intermittency(Sandhaas et al., 2022). The combined load factor is $f_{load}(t) = f_{daily}(t) \cdot f_{weekly}(t)$, with $f_{daily}(t)$ = 1.0 during daytime operating hours (06:00-22:00) and 0.3 during nighttime hours (22:00-06:00), reflecting industrial shift operation. f_{weekly}= 1.0 (weekdays), 0.6 (Saturday), 0.2 (Sunday). Combined f_{load} ranges from 1.0

(weekday daytime) to 0.06 (Sunday night), capturing the strong intermittency that distinguishes industrial sources from the near-continuous WW and DC sources.
For both configurations, source temperature and recoverable heat are:

$$T_{ind,i}(t) = T_{base,i} + \Delta T_i \times f_{load}(t) \quad (20)$$

$$Q_{ind}(t) = Q_{ind,base} \times f_{load}(t) \quad (21)$$

with configuration-specific parameters in Table 5.

Table 5: IWH configuration parameters.

Config.	T_{base}(°C)	ΔT(°C)	Operability
IND-A (high-T)	45	5	Lift = 0-5°C in summer at T_{sup}= 50°C; HP blocked across most shoulders and summer hours. Most demanding test of the minimum-lift constraint.
IND-B (low-T)	30	10	Lift = 10°C in summer (HP blocked at peak load); reaches 30-40°C in winter at T_{sup}= 70°C. Partial year-round operability with blocking confined to warm months at peak industrial load.

Both share $Q_{ind,base}$= 9.25MW, $Q_{HP,nom}$= 14MW, and the same $f_{load}(t)$pattern. Operability assessed against the 15°C minimum HP lift threshold (section 3.3.2) and the 4GLTDH supply range.

3.3.6 Heat Demand Profile Construction

The hourly demand profile Q_{demand}(t) is constructed from the 36GWh annual total (section 3.2.2) through a three-stage disaggregation.

1. **Monthly distribution:** The annual total is distributed by month using national Finnish monthly demand fractions f_{month}, normalized by the number of hours in each month:

$$Q_{month} = \frac{Q_{annual} * f_{m(t)}}{N_{h,m(t)}} \quad (22)$$

Where $m(t)$ is the month index of hour t, $N_{h,m}$ is the number of hours in month m.

2. **Diurnal profile:** A normalized diurnal shape $d(h)$ is constructed using superimposed Gaussian functions centred on the morning (06:00) and evening (17:00) residential demand peaks typical for Finnish DH systems (Lavikainen & Fränti, 2024).

$$d(h) = \frac{0.5+0.65\cdot e^{-\frac{1}{2}\left(\frac{h-6}{1.2}\right)^2} +0.50\cdot e^{-\frac{1}{2}\left(\frac{h-17}{0.9}\right)^2}}{mean(D_h)} \quad (23)$$

Where baseline = 0.5, 0.65 and 0.5 are amplitude values of the peak hours, Gaussian morning and evening widths are 1.2 and 0.9, respectively.

3. **Scaling to annual total:** The seasonal and diurnal factors are combined and scaled to preserve the 36 GWh annual total:

$$Q_{demand}(t) = Q_{month}(t) \times d\big(h(t)\big) \times \frac{Q_{annual}}{\sum_{t=0}^{8759} Q_{month}(t)\cdot d\big(h(t)\big)} \quad (24)$$

The resulting annual profile is shown in Figure 7 confirming the expected seasonal dominance of winter demand and the diurnal double-peak structure (Lavikainen & Fränti, 2024) throughout the heating season.

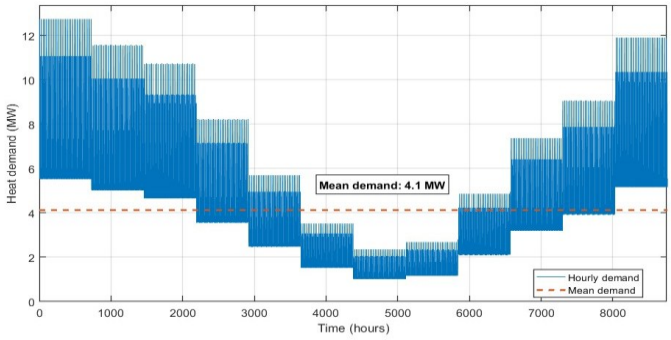

Figure 7: Annual DH demand profile.

3.4 Control Strategies

Two operational control strategies are implemented to investigate how dispatch logic affects the technical, economic, and environmental performance of HP-TES system integration. Strategy 1 is a T-D baseline reflecting existing Nordic DH operational practice, while Strategy 2 (P-D) introduces electricity price awareness to exploit market signals for cost reduction and operational flexibility. Both strategies issue three setpoints at each hourly timestep, which are the HP thermal output $Q_{HP,set}(t)$, TES charging $Q_{ch,set}(t)$, and TES discharging $Q_{dis,set}(t)$, both rely on $Q_{HP,actual}(t)$and $SOC(t)$as feedback signals. Unit-delay blocks on these feedback paths break algebraic loops and reflect real DH

practice, where dispatch decisions use last-interval sensor readings rather than instantaneous feedback.

3.4.1 Strategy 1: Temperature-Driven Control

T-D dispatch is governed entirely by outdoor ambient temperature $T_{amb}(t)$, with system state and seasonal heating need inferred from weather. Three temperature zones partition the year, each combining HP and TES dispatch logic appropriate to that season's thermal regime (Table 6). Zone thresholds are set at T_{low}= −5°C and T_{mid}= 5°C, which correspond to the Vaasa heating-season transitions. Below −5°C, demand can exceed HP nominal capacity and storage support is required while in between −5°C and 5°C, demand is significant but typically within HP capacity. Above 5°C demand decreases through the shoulder season into summer, where surplus production can be diverted to TES charging at high COP.

Table 6: T-D control logic.

Zone	T_{amb} range	Thermal regime	$Q_{HP,set}$	$Q_{ch,set}$	$Q_{dis,set}$
1-Peak winter	$T_{amb} < -5$°C	Heating peak; demand may exceed HP capacity	$Q_{HP,nom}$	0	$Q_{dem}(t)$
2-Normal heating	$-5 \leq T_{amb} \leq 5$°C	Significant but manageable demand	$\min(Q_{dem}, Q_{HP,nom})$	0	$\max(Q_{dem} - Q_{HP,act}, 0)$
3-Recharge	$T_{amb} > 5$°C	Reduced demand through shoulder and summer; high source temperatures and favourable lift give the highest annual COPs	$Q_{HP,nom}$	$\max(Q_{HP,act} - Q_{dem}, 0)$	0

HP and TES setpoints are determined by ambient temperature zone with thresholds T_{low}= −5°C and T_{mid}= 5°C. TES discharge is conditional on $SOC(t) > SOC_{min}$= 0.05; TES charge is conditional on $SOC(t) < SOC_{max}$= 0.95. The peak-winter discharge logic and the recharge surplus-to-storage logic reflect standard Nordic large DH thermal store practice (Lieskoski et al., 2024).

Zone logic reflects the operational role of large DH thermal stores in Nordic systems: TES discharges only during peak winter when demand can exceed HP nominal capacity, and recharges across the warmer half of the year when demand is reduced and source-sink lift is most favourable.

3.4.2 Strategy 2: Price-Driven Control (Flexibility)

P-D dispatch introduces electricity market awareness through three price-based operating modes determined by comparing the hourly day-ahead price $\lambda(t)$against two thresholds (Table 7). The thresholds are calibrated against the 2024 Finnish day-ahead price distribution: λ_{low}= 0.02 €/kWh corresponds to the 30th percentile (capturing hours of abundant renewable generation or low demand) and λ_{high}= 0.0786 €/kWh corresponds to the 80th percentile (capturing peak-price periods when avoiding HP operation is preferable). These percentile-based thresholds are calibrated to the 2024 Finnish day-ahead price distribution and would require recalibration for other years as the renewable generation mix and market conditions evolve. The choice of the 30th and 80th percentiles as the calibration points is itself a design parameter, while the sensitivity analysis in Section 3.5.2 quantifies the impact of varying the resulting threshold values.

Table 7: P-D control logic.

Mode	$\lambda(t)$range	Rationale	$Q_{HP,set}$	$Q_{ch,set}$	$Q_{dis,set}$
Low price	$\lambda \leq \lambda_{low}$	Capture cheap energy, build TES reserve	$Q_{HP,nom}$	$\max(Q_{HP,act} - Q_{dem}, 0)$	0
Mid-price	$\lambda_{low} < \lambda \leq \lambda_{high}$	Demand-following operation	$\min(Q_{dem}, Q_{HP,nom})$	0	$\max(Q_{dem} - Q_{HP,act}, 0)$
High price	$\lambda > \lambda_{high}$	Avoid HP operation, draw from store	0	0	$Q_{dem}(t)$

HP setpoint is determined by price band; TES charge and discharge logic coordinates explicitly around HP operation. Conditional gates: $SOC(t) < SOC_{max}$= 0.95 for charging, $SOC(t) > SOC_{min}$= 0.05 for discharging.

Unlike T-D, where TES discharge is reserved for peak winter, P-D uses the TES as an active arbitrage buffer by charging during low-price hours regardless of season and discharging fully during high-price hours regardless of demand level. This unlocks the load-shifting potential of the storage and exposes the system to higher cycling, with both effects quantified through the KPIs in (section 3.6).

3.5 Scenario Matrix and Sensitivity Analysis

3.5.1 Simulation Scenarios

The simulation study is organized around a structured scenario matrix that progresses from the current 3GDH baseline through a series of 4GLTDH configurations. The three waste heat source categories are examined, each branching into source-specific sub-cases and evaluated under both T-D and P-D control. To ensure full comparability across the matrix, all scenarios share identical external input signals, which are the 2024 Vaasa hourly Finnish day-ahead electricity prices, ambient temperature, hourly CO_2 emission factors, and hourly heat demand profile (36GWh). Each scenario is simulated over a complete calendar year with the TES configuration held constant across all scenarios. The baseline scenario S0 represents the existing Pått 3GDH operation at 95°C supply temperature and serves as the thermodynamic and environmental reference point against which all LTDH scenarios are benchmarked. Table 8 summarizes the complete scenario matrix.

Table 8: Simulation scenario matrix.

ID	Label	Control Strategy	Heat Source	Config	HP Cap. (MW)	T_{source} Range (°C)	Supply Temp. (°C)
S0	Baseline Pått	T-D	WW (Pått)	-	12	10-15	95 (3GDH fixed)
S1a	WW	T-D		-			50-70 (4GLTDH)
S1b	WW	P-D		-			
S2a	DC Secondary	T-D	DC (WSTAR)	DC-S	7.5	37-45	
S2b	DC Secondary	P-D		DC-S			
S2c	DC Primary	T-D		DC-P	6.7	30-35	
S2d	DC Primary	P-D		DC-P			
S2e	DC Air-cooled	T-D		DC-A	3.0	20-30	
S2f	DC Air-cooled	P-D		DC-A			
S3a	Industrial High	T-D	Industrial	IND-A	14	45-50	
S3b	Industrial High	P-D		IND-A			
S3c	Industrial Low	T-D		IND-B		30-40	
S3d	Industrial Low	P-D		IND-B			

Each block of scenarios isolates a specific research question. S0 vs S1a quantifies the thermodynamic and environmental consequences of the 3GDH to 4GLTDH transition for the same WW source (RQ1, RQ4). S1a vs S1b, S2a vs S2b, … isolate the effect of control strategy under identical source conditions (RQ3). S1 vs S2 vs S3 compares the three

waste heat source classes at the LTDH level (RQ1, RQ2). The complete scenario matrix, therefore, enables systematic decomposition of the contribution of source characteristics, network temperature regime, and control strategy to overall system performance.

3.5.2 Sensitivity Analysis Parameters

A one-at-a-time (OAT) sensitivity analysis quantifies the influence of the most consequential parameters on the four headline KPIs (SPF, annual CO_2 emissions, DCR, annual electricity cost) by varying each parameter independently while holding all others at their base-case values. The eight parameters span component sizing, source characterization, control thresholds, and demand assumptions (Table 9). Results are reported in the section 4.5 as tornado charts showing the relative impact of each parameter on each KPI.

Table 9: Sensitivity analysis parameters.

Parameter	Base Value	Low	High	Basis
HP Carnot efficiency factor (η)	0.50	0.40	0.60	Range for large waste-heat compression HPs (Pieper et al., 2019)
TES capacity (E_{max})	470 MWh	250 MWh	720 MWh	Low $\sim 1.9\ days$ and high $\sim 5.4\ days$ span at $P_{max} = 5MW$ and usable capacity (90% of E_{max}), Proportionally scaled from Vaskiluoto TES (Vaasan Voima, 2023).
TES charge/discharge power (P_{max})	5 MW	3 MW	8 MW	Low (3 MW) and high (8 MW) correspond to charge durations of 141h and 53h respectively at base $E_{max} = 470MW$
Low electricity price threshold (λ_{low})	0.02 €/kWh	0.01 €/kWh	0.04 €/kWh	Calibrated to the 2024 Finnish day-ahead price distribution (Transparency Platform, 2026)
High electricity price threshold (λ_{high})	0.079 €/kWh	0.060 €/kWh	0.100 €/kWh	Calibrated to 2024 Finnish day-ahead price distribution(Transparency Platform, 2026)
Annual heat demand (Q_{annual})	36GWh	27 GWh	45 GWh	$\pm 25\%$ reflecting variation in building stock, occupancy, and climate year (Finnish Energy, 2026)
WW source temperature (T_{ww})	12.5°C	10°C	15°C	Operational range of the Påtti facility (Vaasan Vesi, 2024)
Minimum lift threshold ($\Delta T_{lift,min}$)	15°C	10°C	20°C	Practical operability range for large electric compression HPs(Barco-Burgos et al., 2022)

Base values match the configurations of the section 3.3, and ranges reflect documented variation in the literature or operational practice.

3.6 Performance Indicators

System performance is evaluated using twelve quantitative indicators computed from hourly simulation outputs and organized into three categories: technical efficiency,

environmental impact, and operational flexibility (Table 10). All KPIs are computed in a post-processing MATLAB script applied uniformly across all scenarios.

Table 10: Performance indicators.

KPI	Definition	Unit	Category
SPF	Ratio of total annual HP heat output to total annual HP electricity consumption: $SPF = Q_{HP,annual}/Q_{el,annual}$	-	Technical
Mean annual COP	Energy-weighted average of hourly COP when HP is operating: $\frac{\sum[\mathrm{COP(t)}\cdot Q\_{HP,actual}(\mathrm{t})]}{\sum Q\_{HP,actual}(\mathrm{t})}$	-	
Demand coverage ratio	The fraction of annual heat demand met by the combined HP and TES output: $DCR = Q_{satisfied,annual}/Q_{demand,annual}$	%	
HP utilization rate	The fraction of annual hours during which the HP delivers non-zero heat output: $U_{HP} = t_{HP,on}/8760$	%	
HP blocking hours	when the HP is forced off exclusively by the minimum lift constraint rather than by control strategy decision: $U_{lift}(\mathrm{t}) = 0$ (minimum lift gate active)	h/yr	
TES utilization index	Measures the degree to which the TES is actively used relative to its capacity, computed as the sum of annual charge and discharge energy divided by twice the maximum usable capacity: $TUI = \frac{(Q_{charge,annual} + Q_{discharge,annual})}{(2 \times 0.9 \times E_{max})}$	-	Technical, Flexibility
Annual electricity cost	computed by multiplying hourly HP electrical consumption by the hourly day-ahead electricity price: $C_{el} = \sum Q_{el,HP}(t) \times \lambda(\mathrm{t})$	€	Flexibility
Peak electricity demand	Maximum hourly HP electrical power draws over the simulation year: $Q_{el,peak} = \max[Q_{el,HP}(t)]$	MW	
Load shifting potential	Hours per year where Strategy 2 HP setpoint deviates from Strategy 1 by more than 10% of $Q_{HP,nom}$	h/yr	
Annual CO_2 emissions	Associated with HP hourly electrical energy consumption: $E_{CO_2} = \sum Q_{el,HP}(t) \times \mathrm{EF(t)}$, where EF(t) is the hourly grid emission factor	tCO_2	Environmental
CO_2 avoided	Quantifies the emissions reduction achieved by HP integration relative to the baseline scenario S0: $\Delta E_{CO_2} = E_{CO_2,S0} - E_{CO_2,Sx}$	tCO_2	
Specific CO_2 emissions	Normalize annual emissions by annual heat output, enabling comparison across scenarios with different HP capacities and demand coverage ratios: $e_{CO_2} = \frac{E_{CO_2}}{Q_{HP,annual}}$	gCO_2 /kWh	

All quantities are computed over 8,760 hourly simulation timesteps. Hour-level operators apply only when the HP is operating ($Q_{HP}(t) > 0$).

3.7 Model Verification

Full empirical Verification of the simulation model against measured operational data from the case DH network is precluded, as hourly metered data from the Pått HP plant and the sub-network served by it are not publicly available. The validation strategy therefore follows a structured multi-level approach combining component-level cross-checking, energy balance verification, and benchmark comparison against real-world operational data.

Component-level cross-checks. The HP model reproduces COP values within the documented 2-6 range across the modelled supply and source temperature space (Barco-Burgos et al., 2022). The WW source model yields 6.46MW of recoverable heat at the HP evaporator under nominal conditions (mean source temperature 12.5°C, flow rate 206kg/s, minimum extraction temperature 5°C)(Vaasan Vesi, 2024). At the simulated 3GDH-baseline COP of 2.23, this corresponds to a delivered HP capacity of 11.7MW, consistent with the 12MW nominal capacity of the operational Pått plant(Elomatic, 2024; Vaasan Sähkö, 2026) within 2.5%. The TES analytical charge-hold-discharge cycle reproduces the specified standing-loss coefficient $k = 5 \times 10^{-4}\ h^{-1}$ to within 0.05%.

Energy balance verification. The LTDH network energy balance closes to 0.0% in all 13 scenarios by switch-based subsystem construction. The TES internal energy balance closes within 0.1% per scenario; no scenario required exclusion in the results.

Benchmark comparison. The simulated S0 annual HP heat output of 47.1GWh sits between the Pått plant's 2024 first-full-year operational figure of 41GWh of HP-derived heat (Vaasan Sähkö, 2026)and its publicly stated design production target of approximately 60GWh per year(Vaasan Sähkö, 2025). The +14.9% deviation from the 2024 ramp-up year falls within the ±15% target acceptable for system-level modelling at this resolution, and the −21.5% deviation from the design target is consistent with the conservative model assumptions on source recoverable heat and the synthetic demand profile, which together represent the lower bound of the achievable annual output. The 3G-to-4G SPF improvement, which is $SPF_{S0} = 2.23$ to $SPF_{S1a} = 3.74$ provides an independent secondary benchmark, while the analytical Carnot prediction at the supply-temperature levels with η = 0.50 yields a +70.5% improvement, agreeing with the simulated value within 4%.

These three validation levels do not constitute formal calibration but provide concrete evidence that the simulation framework behaves consistently with documented Pått operational performance, established Carnot thermodynamics, and physical conservation laws.

4 Results and Discussion

4.1 HP-LTDH Technical Compatibility Across Waste Heat Sources

This section addresses RQ1 by analysing how supply temperature regime, source temperature, and cooling architecture determine the thermodynamic compatibility of the HP with the 4GLTDH network. The analysis is based on the T-D scenarios, where dispatch decisions reflect purely thermal conditions, isolating source compatibility from market-driven effects. The annual COP time series for all seven T-D scenarios, revealed in Figure 8 with Figure 9, which summarize HP blocking hours and utilization rate, shows a clear source-temperature compatibility gradient.

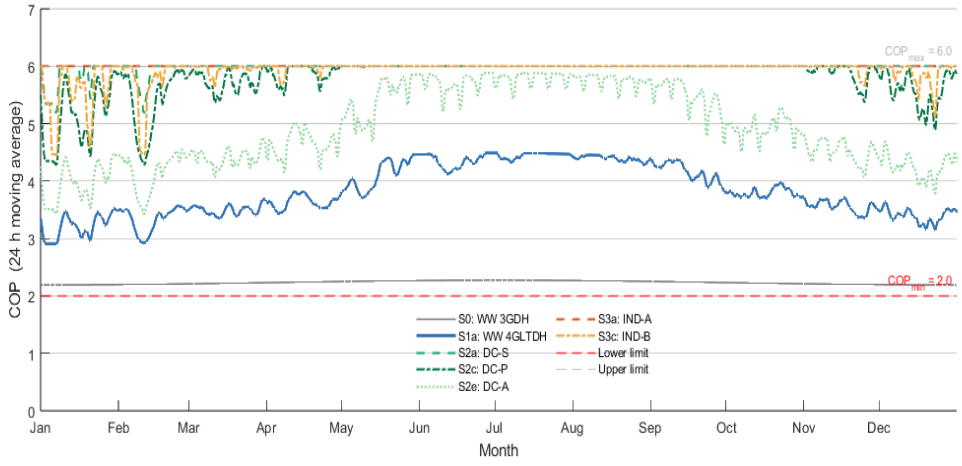

Figure 8: Annual cop time series.

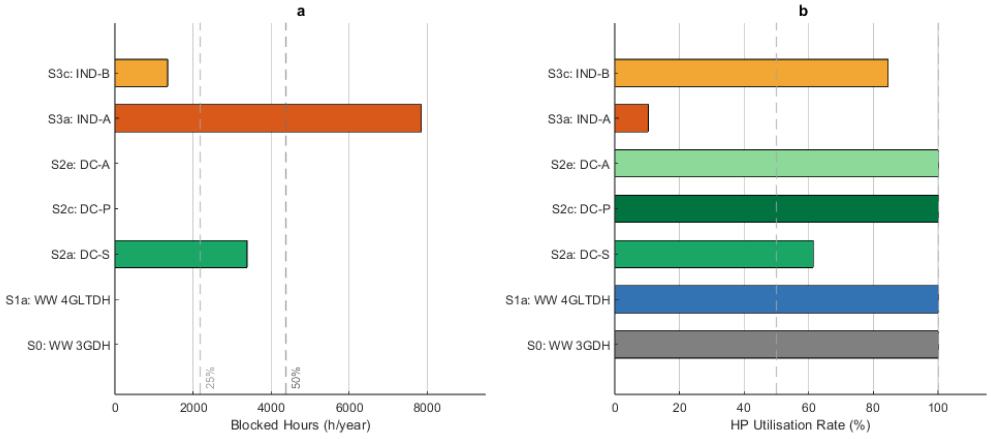

Figure 9: HP technical compatibility by source type: (a) HP blocking hours and (b) HP utilisation rate (% of 8,760 hours).

4.1.1 Effect of Supply Temperature Regime (3GDH to 4GLTDH Transition)

The most fundamental performance shift in the entire scenario matrix occurs between S0 and S1a. Figure 8 illustrates the WW COP rising from a narrow flat band around 2.23 in S0 to a seasonally fluctuating profile of 3.0-4.6 in S1a, mainly due to the reduction in supply temperature to the 4GLTDH curve.

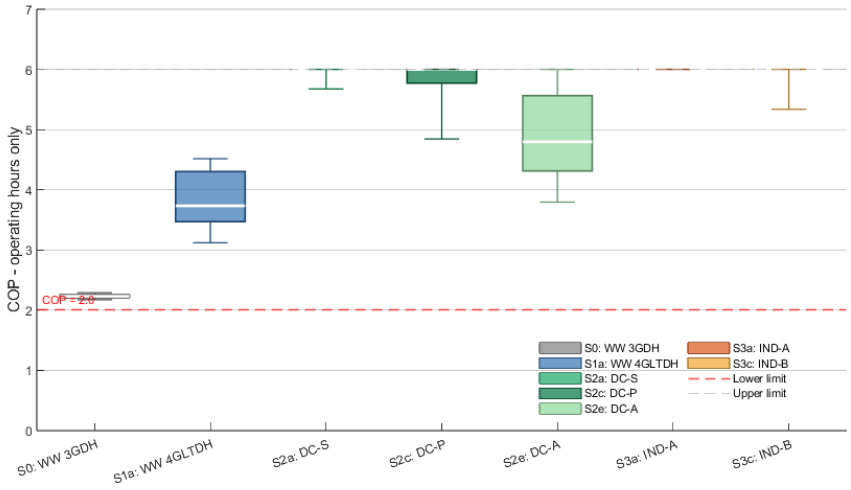

Figure 10: COP distribution by source type (5th-95th percentile).

Figure 10 confirms the distribution shift. The median COP rises from 2.23 to 3.73, and the 5th percentile rises from 2.17 to 3.30. Neither scenario experiences any blocking (Figure 9), confirming that the WW source maintains adequate lift margin year-round under both supply regimes. The SPF improvement from 2.23 to 3.74 quantifies the full thermodynamic benefit of the 3GDH-to-4GLTDH transition for this source.

4.1.2 DC and Industrial Source Compatibility

Figure 11 shows the T_{source} vs COP scatter for all three DC and the two IWH configurations and explains the compatibility differences. DC-S clusters in the upper-right part of the scatter, combining a high source temperature with a high COP. The consequence is shown in Figure 9, which is due to 3,386 blocked hours per year (38.7%), the highest of any non-industrial source, as the source temperature regularly closes the lift margin against the 50°C summer supply floor. By contrast, DC-P shifts left in the scatter. It maintains comparably high COP (mean 5.75) while eliminating blocking entirely (100% utilisation). DC-A sits furthest left, with the widest COP spread as shown in Figure 10 reflecting strong seasonal sensitivity with zero blocking hours like that of DC-P. The three DC

configurations trace a clear trade-off visible across Figure 9: lower extraction temperature increases the lift margin and improves operability at the cost of reduced heat quantity and COP.

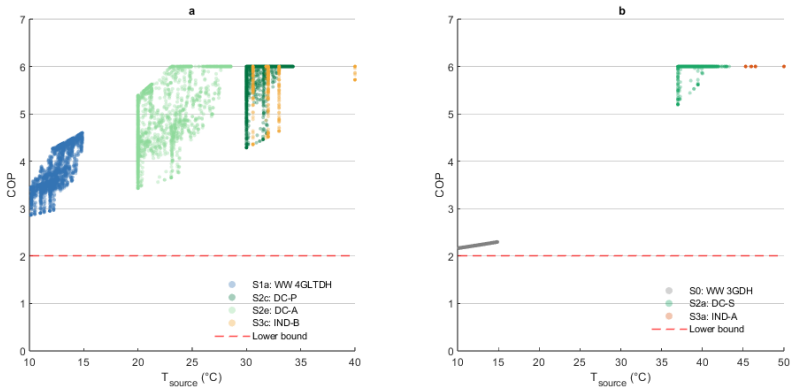

Figure 11: Source temperature vs instantaneous COP (T-D scenarios): (a) lower-temperature sources and (b) higher-temperature sources.

The two industrial configurations frame the extremes of this compatibility gradient. IND-A is blocked for 7,854 hours per year and therefore appears only as a very small bar in Figure 9. Its COP line in Figure 8 appears only as short winter peaks, clamped at 6.00 throughout its 907 annual operating hours. The resulting 7.7% demand coverage confirms that a 45-50°C industrial source is thermodynamically incompatible with 4GLTDH HP integration for all practical purposes. IND-B more favourable behaviour. It maintains a continuous operating COP of 5.7-6.0 through winter with a summer gap of 1,350 hours (15.4% of the year), and its COP distribution remains tightly concentrated near the upper limit. The 84.6% utilization and 61.6% demand coverage confirm that the 30-40°C industrial range is viable for 4GLTDH integration.

4.1.3 Source Temperature Compatibility Gradient

Table 11 and Figure 9 establish a clear source temperature compatibility gradient across the full scenario matrix. Sources with mean temperature lift above 33°C (WW, DC-P, and DC-A), achieve full year-round HP operability at 84-100% utilisation. Sources with mean lift of 21-25°C such as DC-S, and IND-B experience partial blocking of 15-39% of annual hours concentrated in warm months, with demand coverage ranging from 61.6% to 88.6% depending on heat capacity. In contrast, sources with mean lift below 20°C (IND-A) are

blocked for about 90% of the year and cannot serve as viable primary HP sources under 4GLTDH conditions.

The main limiting factor throughout is the 4GLTDH summer supply temperature floor of 50°C. Any source whose temperature approaches or exceeds 35°C will trigger the minimum lift gate during warm months practically. This directly answers RQ1 as: HP-4GLTDH technical compatibility requires either a source temperature consistently below approximately 35°C, or a supply temperature flexibility that maintains lift above 15°C year-round. Among the configurations studied, WW and DC-P and DC-A satisfy this condition fully or nearly fully; DC-S and IND-B streams satisfy it partially; and IND-A source do not satisfy it under the modelled 4GLTDH operating conditions.

Table 11: HP technical compatibility (T-D scenarios).

Scenario	T_{source} mean (°C)	Mean lift (°C)	SPF	Blocked (h/yr)	U_{HP} (%)	DCR (%)
S0 WW	12.5	82.5	2.23	0	100.0	99.7
S1a WW	12.5	43.7	3.74	0	100.0	96.9
S2a DC-S	38.1	21.3	5.95	3,386	61.4	67.8
S2c DC-P	31.2	25.0	5.71	0	100.0	88.6
S2e DC-A	22.4	33.9	4.76	0	100.0	50.7
S3a IND-A	46.7	18.6	6.00	7,854	10.4	7.7
S3c IND-B	34.2	23.0	5.92	1,350	84.6	61.6

4.2 Source-Dependent HP Efficiency and Annual Heat Contribution

This section addresses RQ2 by comparing annual efficiency and heat contribution across source types under T-D control strategy. Figure 12 presents the SPF results in two views: the absolute SPF per scenario (a) and the SPF-Source mean temperature relationship (b).

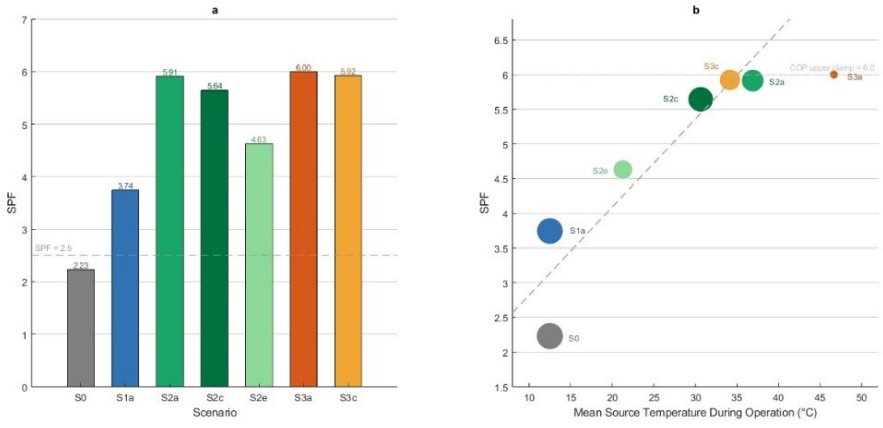

Figure 12: a) SPF and (b) SPF vs. Mean source temperature T-D scenarios (bubble size ∝ DCR).

4.2.1 SPF Across Source Types

Source temperature is the dominant driver of SPF. The progression from WW at 12.5°C (SPF 3.74) through DC-A at 22.4°C (SPF 4.76), DC-P at 31.2°C (SPF 5.71), IND-B at 34.2°C (SPF 5.92), and DC-S at 38.1°C (SPF 5.95) follows the Carnot relationship closely as shown on Figure 12 a and b. Higher source temperatures reduce the temperature lift and raise COP toward the upper clamp of 6.0. IND-A (46.7°C, SPF 6.00) is an apparent outlier. its SPF reaches the clamp precisely because the HP operates only 907 hours annually, exclusively during winter conditions where maximum lift is available. This illustrates the fundamental distinction between instantaneous efficiency and system-level performance that happens throughout the analysis.

4.2.2 Annual Heat Contribution and Efficiency-Coverage Balance

Figure 13 reveals that SPF and system contribution are inversely related across source types. The WW source (S1a) delivers 43,592 MWh annually covering 96.9% of the 36 GWh demand, operating year-round without blocking. DC-P delivers 35,520 MWh (88.6% DCR) despite a higher SPF of 5.64 while the slight shortfall relative to WW reflects its smaller heat capacity. DC-S (68.8%), IND-B (61.6%), and DC-A (50.4%) deliver progressively less heat as blocking hours and smaller source capacities limit annual output. IND-A's 2,659 MWh (7.7% DCR) represents the highest SPF in the matrix but the lowest practical contribution, leaving 33,399 MWh of annual demand unmet.

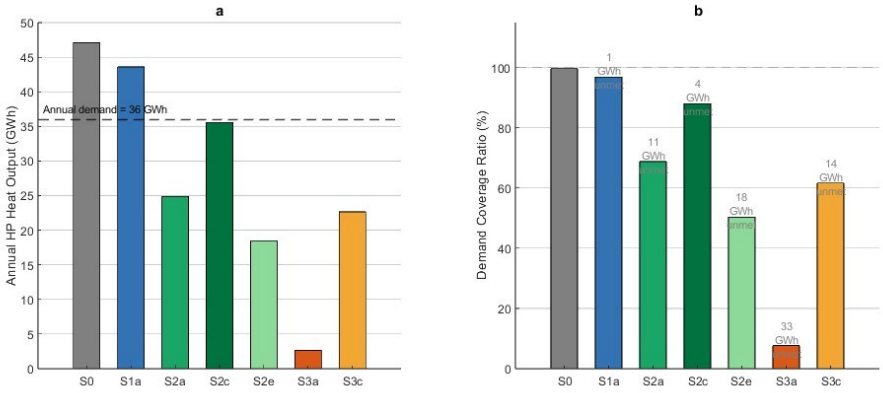

Figure 13: (a) annual HP heat contribution and (b) demand coverage (T-D scenarios).

Among all configurations, DC-P achieves the best balance of efficiency and coverage with 5.64 SPF and 88.1% demand coverage and only 4,458 MWh unmet annually. It is the only

non-WW source that approaches near-complete demand coverage while maintaining high efficiency. Figure 12b summarizes the central finding of RQ2 as a source temperature drives SPF upward but drives annual heat contribution downward through increased blocking and smaller heat capacity. The WW source delivers the highest annual contribution despite the lowest SPF among 4GLTDH scenarios, because it operates without interruption year-round. Higher-temperature sources achieve superior instantaneous efficiency but at the cost of reduced supply reliability. For the Vaasa deployment context, DC-P represents the most efficient alternative source that maintains near-WW-level demand coverage, while IND-B offers a viable industrial option at lower DCR but comparable SPF.

4.3 Operational Strategies and Flexibility

This section addresses RQ3 through a comparative analysis of Strategy 1 (T-D) and Strategy 2 (P-D) for each source configuration. The analysis examines whether price-responsive dispatch reduces electricity cost and shifts peak demand without unacceptable degradation of supply reliability. Figure 14 shows the four KPIs that summarize the strategy comparison: SPF, DCR, electricity cost, and TES utilization index.

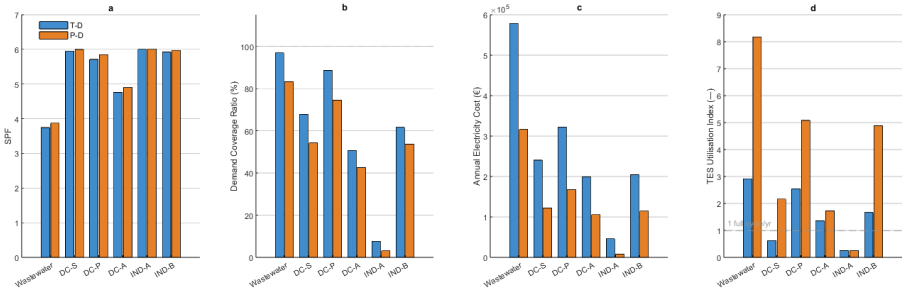

Figure 14: Control strategy comparison: T-D vs P-D.

4.3.1 Cost, SPF, and TES Cycling

P-D dispatches achieve substantial electricity cost reductions across all active source configurations (Figure 14c). The reduction ranges from 44.1% for IND-B, where annual electricity cost falls from €204k to €114k, to 83.0% for IND-A (€46k to €7.8k). WW, DC-S, DC-P, and DC-A also show a reduction of 44-50% (45.3%, 49.2%, 48.1%, and 47.1%,

respectively). This indicate that the Finnish day-ahead price structure consistently enables significant cost arbitrage across source types when the HP can be dispatched flexibly.

SPF results under P-D shows smaller but consistent improvements (Figure 14a). DC-P improves from 5.71 to 5.85, WW from 3.74 to 3.87, and DC-A from 4.76 to 4.90, corresponding to gains of about 0.13-0.14. This reflects preferential HP operation during low-price hours that coincide with more favourable temperature conditions.

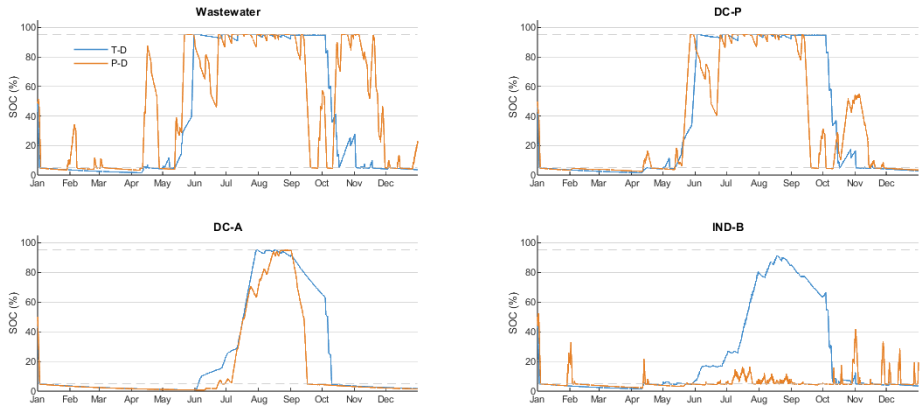

Figure 15: Annual TES state of charge: T-D vs P-D Strategy.

Figure 15 provides the most visually distinctive result of the strategy comparison. For WW, the T-D SOC profile follows a gradual seasonal pattern by slowly discharging through winter, recharging in spring and summer while the P-D profile shows aggressive large-amplitude cycling throughout the year as the TES is repeatedly charged during low-price hours and discharged during high-price periods. This drives TUI from 2.92 to 8.18 which is the largest increase in the scenario matrix, representing approximately 2.8 additional full usable cycles per year and 4,198MWh of annual TES charging versus 1,548MWh under T-D.

DC-P shows TUI increases from 2.55 to 5.08, with annual TES charging more than doubling from 1,374 to 2,603MWh as shown on Figure 15 and Figure 14d. IND-B shows a similar pattern with TUI rising from 1.67 to 4.88. DC-A shows only a modest TES cycling increase (1.36 to 1.72), reflecting the smaller HP capacity limiting the energy available for arbitrage. IND-A shows no change in TES behaviour under either strategy (TUI = 0.25

in both) since the HP operates so rarely that neither the price signal nor the temperature signal meaningfully alters its dispatch.

4.3.2 Supply Reliability and Peak Demand

P-D consistently reduces demand coverage across all source configurations with the severity depending on HP capacity and source operability, as shown on Figure 14b. The largest absolute reliability penalty occurs in DC-P as unmet demand increases from 4,249MWh (11.8%) under T-D to 9,351MWh (26.0%) under P-D. That is equivalent with the increase of 5,102MWh, which is the largest in the scenario matrix. Figure 16b makes this visible in the monthly profile. DC-P January heat satisfied drops from 4,058MWh under T-D to 1,944MWh under P-D (a 52% reduction in the coldest month) as P-D cutting back coincides with peak winter demand.

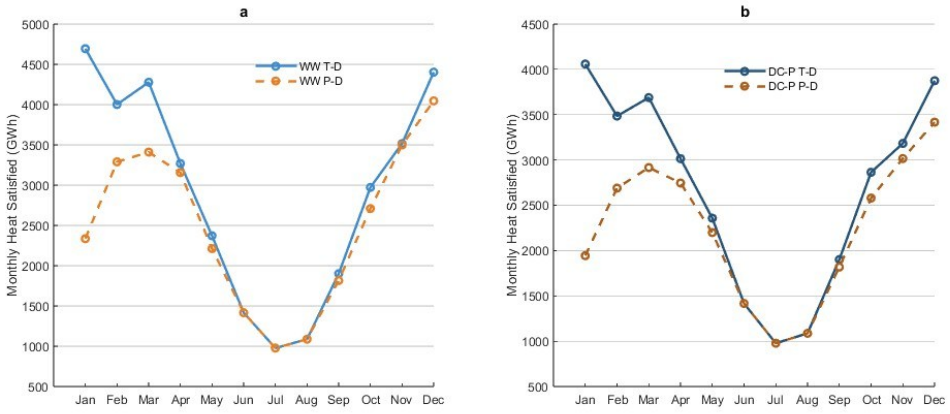

Figure 16: T-D vs P-D monthly heat satisfied: (a) WW and (b) DC-P.

The WW scenario shows a similar pattern on Figure 16a. January heat drops from 4,694MWh to 2,335MWh (−50%), and annual unmet demand rises from 1,269MWh (3.5%) to 6,203MWh (17.2%). For lower-coverage sources, the absolute penalty is smaller: DC-A adds 2,939MWh unmet (+8.2 pp), and IND-B adds 2,892MWh (+8.0 pp). IND-A has an additional 1,643MWh unmet under P-D of its already near-total supply gap of 33,399MWh.

Peak electricity demand reductions under P-D are smaller across all source types (Figure 17a). DC-S achieves the largest reduction (−5.4%), followed by WW (−4.6%) and DC-A (−4.5%). DC-P shows the smallest reduction (−1.8%) and IND-A shows none. The limited

peak reduction reflects the fact that the highest-price hours in Finland which trigger HP curtailment under P-D are concentrated in cold winter periods when demand is highest, so the HP is simultaneously needed most and curtailed most aggressively.

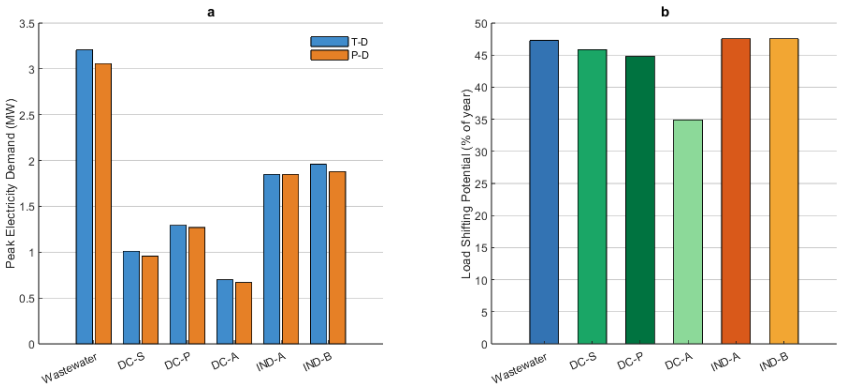

Figure 17: Flexibility performance of P-D dispatch: (a) peak electricity demand reduction and (b) load shifting potential.

Load shifting potential ranging from 3,059 hours (DC-A, 34.9% of the year) to 4,165 hours (IND-A and IND-B, 47.5%) (Figure 17b). However, IND-A's high LSP reflects near-zero T-D setpoints throughout the year (any small P-D deviation registers as shifting). The more meaningful LSP values are WW (4,143h, 47.3%), DC-S (4,018h, 45.9%), and DC-P (3,923h, 44.8%), all of which represent genuine dispatch reorganization relative to a high-coverage T-D baseline.

4.3.3 Cost-Reliability Balance

P-D dispatch achieves electricity cost reductions of 44-50% across all operational sources but introduces a supply reliability penalty in every case except IND-A, where the HP barely operates under either strategy. The cost-reliability balance is most critical for the highest-coverage sources such as WW and DC-P, that achieve the best T-D coverage but experience the largest P-D unmet demand increases, because of the fact that the P-D curtailment strikes precisely during cold, high-demand periods. Lower-coverage sources like DC-A and IND-B accept smaller absolute reliability penalties for comparable percentage cost savings, suggesting a more favourable cost-reliability balance for these configurations in a system with auxiliary backup capacity.

The TES plays a central role in mediating this trade-off. Sources with high TUI under P-D use storage more intensively to partially buffer the reliability loss from HP curtailment, but the 470MWh TES capacity is insufficient to fully compensate for curtailment during multi-day cold spells. A larger TES or lower price thresholds shift the balance toward better reliability preservation under P-D. This interaction is examined in the sensitivity analysis in section 4.5.

Table 12: Control strategy comparison-KPI summary.

Source	SPF (T-D/P-D)	DCR% (T-D/P-D)	Cost €k (T-D/P-D)	Cost red. (%)	Unmet MWh (T-D/P-D)	TUI T-D/P-D
WW	3.74 / 3.87	96.9 / 83.2	579 / 316	−45.3	1,269 / 6,203	2.92 / 8.18
DC-S	5.95 / 6.00	67.8 / 54.2	240 / 122	−49.2	11,748 / 16,628	0.63 / 2.16
DC-P	5.71 / 5.85	88.6 / 74.5	322 / 167	−48.1	4,249 / 9,351	2.55 / 5.08
DC-A	4.76 / 4.90	50.7 / 42.5	199 / 106	−47.1	17,912 / 20,851	1.36 / 1.72
IND-A	6.00 / 6.00	7.7 / 3.1	46 / 8	−83.0	33,399 / 35,042	0.25 / 0.25[1]
IND-B	5.92 / 5.97	61.6 / 53.6	204 / 114	−44.1	13,968 / 16,860	1.67 / 4.88

4.4 Environmental Performance

This section addresses RQ4 by analysing annual CO_2 emissions, CO_2 avoided relative to the S0 baseline, specific emissions per unit heat delivered, and electricity cost across all scenarios.

4.4.1 Annual and Specific CO_2

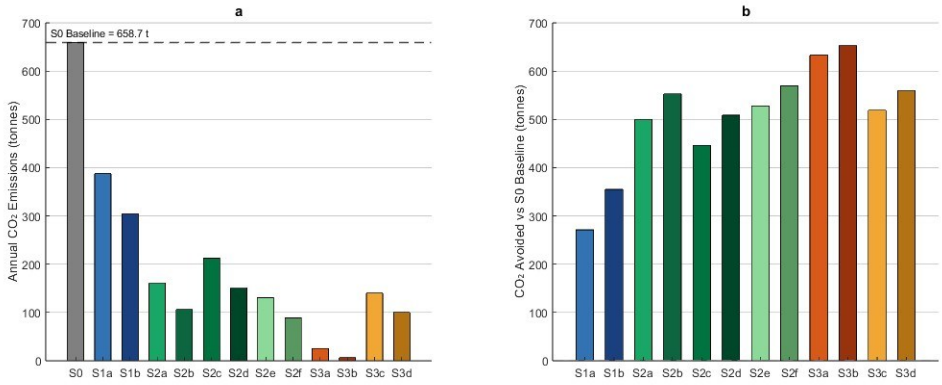

Figure 18: Annual CO_2 emissions and avoidance of all scenarios.

[1] IND-A values should be interpreted with caution. The HP operates just 907 hours annually (10.4% utilization), covering 7.7% & 3.1% of demand. The −83% cost reduction is therefore driven by extremely low absolute values rather than efficient price-responsive dispatch and cannot be meaningfully compared to the 44-49% reductions achieved by the higher-utilization sources. It is unsuitable as a primary heat source and its percentage KPIs are reported for completeness only.

Annual CO_2 emissions declining sharply from the S0 baseline of 658.7 tonnes across all LTDH scenarios (Figure 18a). The 3GDH-to-4GLTDH transition alone represented by S1a reduces emissions by 271.1 tonnes (41.2%) through SPF improvement from 2.23 to 3.74, consuming proportionally less electricity for the same heat output. Further reductions follow as source temperature rises and SPF increases. Under the T-D dispatch, DC-S reaches 159.8t (−75.7% vs S0) while DC-P is 212.2t (−67.8%), DC-A is 130.5t (−80.2%), and IND-B reaches 140.0t (−78.8%). IND-A T-D achieves the lowest absolute emissions of all T-D scenarios at 25.8t (−96.1%), which is a consequence of operating only 907 hours annually rather than pure decarbonisation of the full demand.

Figure 18b shows that CO_2 avoided is influenced by both SPF and annual operating hours. The top scenarios by CO_2 avoided are IND-A under both P-D and T-D (99.0% and 96.1% of S0 baseline respectively), followed by DC-A P-D (86.5%), IND-B P-D (84.8%), and DC-S P-D (83.9%). However, the IND-A avoidance of nearly all S0 emissions is achieved because the HP barely operates, meaning the network relies on unmodelled auxiliary sources for 92.8% of demand rather than the HP itself. The most meaningful avoided CO_2 values combine high avoidance with adequate demand coverage. DC-P P-D (508.6t avoided, 74.5% DCR) and DC-P T-D (446.5t, 88.6%) represent the strongest genuine decarbonisation contributions among configurations that also deliver reliable heat supply.

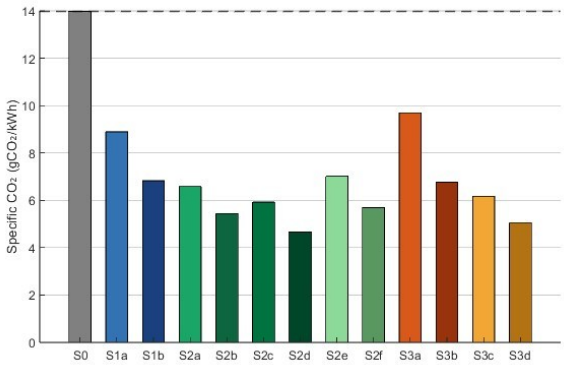

Figure 19: Specific CO_2 emissions per heat unit.

Specific CO_2 emissions normalize for annual heat output and reveal the per-unit-heat carbon efficiency of each configuration (Figure 19). The S0 baseline of 13.98 gCO_2/kWh is the highest in the matrix. The 4GLTDH transition reduces this to 8.89 gCO_2/kWh for WW T-D (36% reduction). Among T-D scenarios, DC-P achieves the lowest specific

emissions at 5.93 gCO_2/kWh, followed by IND-B (6.18), DC-S (6.58), and DC-A (7.01). IND-A T-D's specific emissions of 9.70 gCO_2/kWh are paradoxically high despite its near-zero absolute emissions since the HP operates only during winter cold snaps when grid CO_2 intensity and electricity prices are both elevated. So, the small amount of electricity it consumes is disproportionately grid-carbon-intensive. P-D dispatch reduces specific emissions across all sources. The largest reductions occur for IND-A (9.70 to 6.77 gCO_2/kWh), WW (8.89 to 6.83), and DC-P (5.93 to 4.66). DC-P P-D achieves the lowest specific emissions in the entire matrix at 4.66 gCO_2/kWh, confirming it as the most carbon-efficient configuration on a per-unit-heat basis.

4.4.2 P-D as a Carbon Co-Benefit

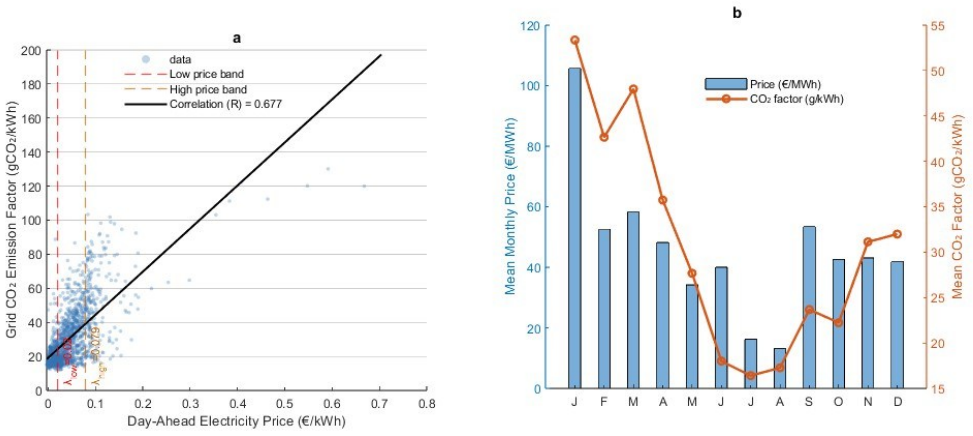

Figure 20: Electricity price vs. grid CO_2 factor - 2024 Finnish market: (a) hourly price vs. CO_2 emission factor and (b) monthly mean price and CO_2 factor.

Figure 20a reveals the mechanism behind P-D CO_2 reductions. Low-price hours (≤0.02 €/kWh, 2,828 hours) carry a mean grid CO_2 factor of only 19.6 gCO_2/kWh which is 62% lower than high-price hours (≥0.079 €/kWh, 1,433 hours) at 52.1 gCO_2/kWh. The Pearson correlation between hourly price and CO_2 factor is R = 0.677, which is a strong positive relationship confirming that the price signal is a reliable proxy for grid carbon intensity. Figure 20b shows this pattern clearly at monthly resolution: winter months combine high prices with high CO_2 factors while summer months show both near-zero prices and low CO_2 factors, driven by high renewable generation shares.

By preferentially operating the HP during low-price hours, Strategy 2 simultaneously reduces electricity cost and grid carbon intensity (a genuine dual co-benefit). Figure 18a

confirms this across all source pairs. P-D reduces absolute CO_2 by 19.5-83.8 tonnes depending on the source. The largest absolute CO_2 reduction under P-D occurs for WW (−83.8 t) due to its large operating volume, though the largest percentage reduction occurs for IND-A (−75.7%) due to its extreme sensitivity to the few hours it operates.

4.4.3 Joint CO_2 vs Cost Performance

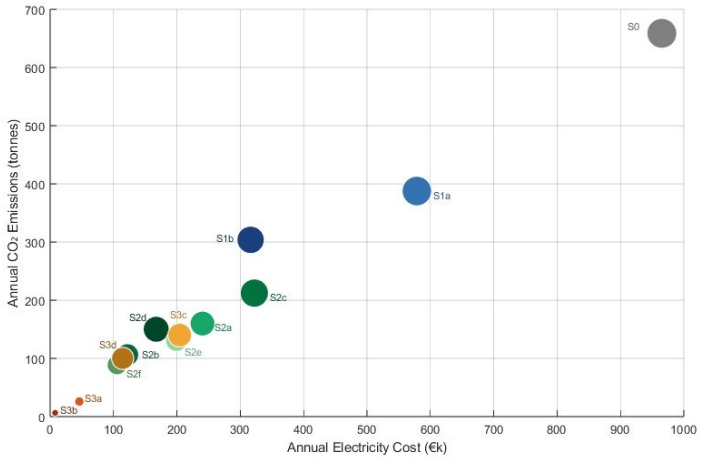

Figure 21: CO_2 emissions vs. electricity cost (bubble size ∝ DCR).

Figure 21 plots all scenarios as a CO_2-cost scatter with bubble size proportional to DCR. The scenarios minimizing both cost and CO_2 are traced by DC-A P-D, DC-S P-D, and IND-B P-D in the lower-left. DC-P P-D offers the most balanced position: lowest specific emissions (4.66 gCO_2/kWh), moderate cost (€167k), and 74.5% DCR. S0 occupies the far upper right at €965k and 658.7t, confirming that any 4GLTDH HP integration delivers both environmental and economic improvement over the 3GDH baseline.

The net decarbonisation effect is maximised when high SPF, high annual operating hours, and P-D dispatch align, which is a condition most completely satisfied by DC-P P-D (SPF 5.85, 83.5% HP utilisation, and the lowest specific emissions in the matrix). WW T-D, despite its lower SPF, achieves meaningful absolute CO_2 reduction (271.1t, 41.2%) through near-complete year-round operation. This confirms that source operability is as important as instantaneous efficiency for total decarbonisation impact.

4.5 Sensitivity Analysis Results

A OAT sensitivity analysis quantifies how eight model parameters defined in section 3.5.2 propagate to the four headline KPIs (SPF, DCR, CO_2, and electricity cost) for three representative scenarios spanning the source matrix, which are WW (the highest-coverage continuous source), DC-A (a partial-coverage data center source), and IND-B (a lift-constrained intermittent industrial source). Figure 22 presents tornado charts for all 12 scenario-KPI combinations, with each panel sorted independently by parameter swing. Table 13 summarises the dominant parameters per KPI as the maximum percentage deviation from each scenario's base-case value.

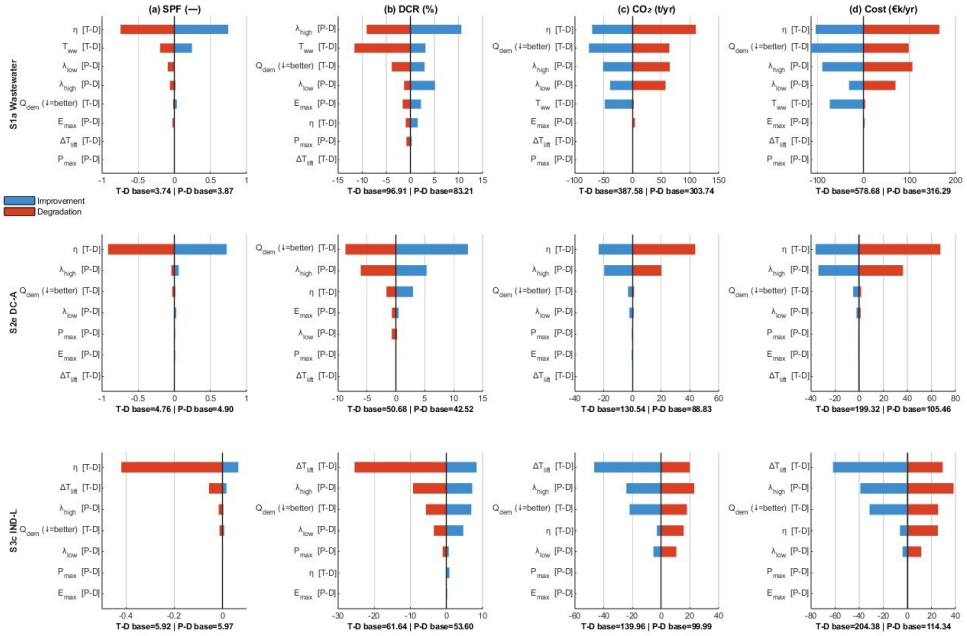

[T-D] = evaluated on T-D base | [P-D] = evaluated on P-D base | T_{ww} applies to wastewater only | Q_{dem} (↓=better): lower demand

Figure 22: Sensitivity Analysis-Tornado Charts (OAT).

Table 13: Dominant sensitivity parameters - maximum percentage deviation from base.

KPI	Most sensitive	WW	DC-A	IND-B	Second	WW	DC-A	IND-B
SPF	η	$\pm 20\%$	$\pm 19\%$	$\pm 7\%$	T_{ww}	$\pm 7\%$	-	-
DCR	$T_{\text{ww}}, Q_{\text{demand}}, \Delta T_{\text{lift}}$	$\pm 12\%$	$\pm 25\%$	$\pm 41\%$	λ_{high}	$\pm 13\%$	$\pm 14\%$	$\pm 17\%$
CO_2	$\eta, \lambda_{\text{high}}$	$\pm 29\%$	$\pm 34\%$	$\pm 33\%$	$\lambda_{low}, Q_{\text{demand}}$	$\pm 20\%$	$\pm 2\%$	$\pm 16\%$
Cost	λ_{high}	$\pm 34\%$	$\pm 35\%$	$\pm 34\%$	η	$\pm 29\%$	$\pm 34\%$	$\pm 12\%$

Three findings emerge from Figure 22 and Table 13. First, SPF is governed almost entirely by the Carnot efficiency factor η, varying from 0.40 to 0.60, which produces deviations

of ±19.9% for WW (SPF 3.74 to 3.00-4.49), ±19.3% for DC-A (4.76 to 3.84-5.48), and ±7.1% for IND-B (5.92 to 5.50-5.99). The reduced IND-B sensitivity reflects near-clamped COP operation, thus changes in increased η have diminishing effects. The WW source temperature T_{ww} contributes a secondary SPF effect of ±6.5% for WW only, confirming that seasonal source temperature variation at the Pått i facility introduces limited but non-negligible efficiency uncertainty. All other parameters produce deviations below 2.5%, confirming that SPF is insensitive to dispatch logic and storage sizing.

Second, DCR shows the most distributed sensitivity profile across all three scenarios. ΔT_{lift} dominates for IND-B at ±41.3%, confirming that this source operates close to the HP blocking boundary and is uniquely sensitive to operability assumptions. For WW, T_{ww} (±12.0%) and λ_{high} (±12.7%) are co-dominant, while Q_{demand} dominates for DC-A (±24.6%) due to its lower base coverage (50.7%). The same HP output satisfies a proportionally larger or smaller fraction of demand depending on the annual demand total, making DCR mechanically sensitive to demand scaling for capacity-limited sources.

The price thresholds λ_{high} and λ_{low} affect DCR across all three scenarios through their control of HP curtailment hours, with λ_{high} producing larger effects (±12.7-17.3%) than λ_{low} (±6.2-8.7%). $E_{\max}$ produce small but non-zero DCR deviations under P-D dispatch (up to 2.6% for WW), while P_{max} produces up to 2.0% for IND-B, both confirming that TES sizing constrains supply adequacy only when price arbitrage actively cycles storage to its capacity and power limits.

Third, CO_2 and cost are co-dominated by η and λ_{high}. η produces ±28.5% CO_2 for WW due to year-round operation, while λ_{high} produces consistent ±21-24% across all three sources, confirming dispatch timing relative to grid carbon intensity is a universal determinant of emissions. ΔT_{lift} produces ±33.4% CO_2 for IND-B, consistent with its large DCR effect since fewer operating hours reduces total electricity consumption proportionally.

Cost mirrors CO_2 in structure but with larger magnitudes. $\lambda_{high}$is the largest cost driver across all scenarios (±33.5%, ±34.5%, ±34.1%), confirming that high-price-threshold calibration is the most consequential operational decision under P-D dispatch regardless of

source type. E_{max} and P_{max} show negligible CO_2 and cost sensitivity (below 1.4%) even under P-D, confirming that TES sizing affects supply coverage but not the carbon or cost intensity of dispatched electricity.

The two modelling assumptions most warranting attention in real-world deployment are therefore uncertainty in real-machine Carnot efficiency (driving SPF and CO_2) and price-threshold calibration (driving cost and CO_2 under P-D). For IND-B specifically, the HP minimum lift threshold $\Delta T_{lift,min}$ is an additional critical uncertainty that should be explicitly addressed in any deployment decision.

4.6 Comparison with Literature

The modelled SPF values of 3.74-6.00 are consistent with the COP range of 2-6 reported for centrally integrated large HPs in 4G and 5G networks by (Barco-Burgos et al., 2022) and with the thermodynamic performance maps reviewed by (Pieper et al., 2019). The WW T-D|P-D results (SPF 3.74|3.87) falls within the 3.0-4.5 range reported for large-scale WW HPs in Scandinavian systems(David et al., 2017), and the DC sources result of SPF 4.76-5.95 is consistent with the 3.0-6.3 COP range reported for DC waste heat integrations (Wahlroos et al., 2017). The modelled 3G-to-4G SPF improvement from 2.23 to 3.74 for WW mirrors the improvement reported by (Averfalk & Werner, 2017) for the equivalent transition in the 4GLTDH framework, validating the thermodynamic assumptions of the model.

The cost and environmental results also compare favourably with reported values. The simultaneous cost-CO_2 co-benefit under P-D is consistent with analyses of Nordic electricity markets where price and grid carbon intensity are positively correlated (Vaissalo et al., 2024). The R = 0.677 price-CO_2 correlation observed in the 2024 Finnish market data is consistent with the structural link between fossil-fuel peaking plant dispatch and high prices documented in Finnish market studies(Energiateollisuus ry, 2025). The TES role in decoupling HP production from demand-central to the P-D strategy is consistent with the flexibility benefits described by (Guelpa & Verda, 2019) and (Christensen et al., 2024).

This finding, together with the quantified cost-reliability balance under P-D dispatch and the differential TES sizing implications between different sources, represents the principal contribution of this thesis to the existing literature on HP-LTDH integration.

5 Conclusions

5.1 Summary of Findings

In relation to RQ1, technical compatibility follows a three-level source-temperature gradient. WW, DC-P, and DC-A, with source temperatures in the 12-32°C range, operate year-round with zero blocking and 84-100% utilization. DC-S (38.1°C) and IND-B (34.2°C) operate partially, blocked for 15-39% of the year when source temperatures approach the 50°C summer supply floor. IND-A (46.7°C) is thermodynamically incompatible since it is blocked for 89.7% of the year, covering only 7.7% of demand (T-D based). The binding compatibility threshold is about 35°C, while COP values across viable scenarios range from 3.74 to 5.95.

In response to RQ2, source temperature is the dominant drive of HP efficiency and annual heat contribution. DC-P T-D achieves the best balance of high efficiency (SPF of 5.71) and high demand coverage (88.6%), making it the highest-performing T-D configuration overall. Among all thirteen scenarios, DC-P P-D achieves the lowest specific CO_2 emissions (4.66gCO_2/kWh) and a strong demand coverage of 74.5%, confirming it as the most thermodynamically efficient and environmentally favourable configuration in the matrix. WW T-D achieves the highest DCR (96.9%) due to its continuous year-round operability, confirming that source availability is just as important as source temperature when assessing annual performance.

In response to RQ3, P-D dispatch consistently reduces electricity cost by 44-83% and CO_2 emissions by 22-76% relative to T-D dispatch across all source types. This makes it deliver a genuine dual co-benefit driven by the positive correlation between Finnish day-ahead electricity prices and grid carbon intensity. However, P-D reduces supply reliability in every case, with unmet demand increasing by 1,643-5,102 MWh depending on source type. The penalty is largest for the highest-coverage sources such as WW (-13.7 pp DCR) and DC-P (-14.1 pp DCR) because near-continuous T-D operation leaves no dispatch headroom. P-D is therefore most suitable for low-to-medium coverage sources operating

alongside auxiliary backup capacity, rather than as a standalone primary heat supply strategy.

In response to RQ4, all 4GLTDH HP integration scenarios reduce annual CO_2 emissions relative to the 3GDH baseline of 658.7 tonnes, with reductions ranging from 41.2% (WW T-D) to 99.0% (barely operating IND-A P-D). The net decarbonization effect is maximized when high SPF, high annual operating hours, and P-D dispatch align simultaneously, that is a condition most completely satisfied by DC-P P-D. The 3GDH-to-4GLTDH transition alone delivers a 41.2% CO_2 reduction through SPF improvement, confirming that supply temperature lowering is a prerequisite for meaningful decarbonization independent of source or control strategy choice.

5.2 Main Contributions

This thesis makes three contributions to the knowledge base on HP integration in Nordic LTDH systems.

A dynamic Simulink modelling framework for HP-LTDH systems. A modular hourly simulation model was developed representing a central large-scale electric HP, three waste heat source categories with realistic temperature profiles, a TES unit, weather-compensated supply temperature control, and Finnish 2024 day-ahead electricity price and grid CO_2 signals. The framework enables full-year dynamic performance assessment under both T-D and P-D dispatch, going beyond the steady-state and component-level analyses that dominate the existing literature. The model is directly parameterized on Vaasa infrastructure data (Påtti WW treatment, WSTAR DC, and Vaskiluoto TES), making the results directly relevant for real operational decision-making.

A quantified multi-source comparison under dual control strategies. Thirteen scenarios spanning three source types, multiple HP configurations, and two control strategies were evaluated against four KPIs within a consistent modelling framework. These findings provide actionable guidance for source selection and operational strategy design in Vaasa and comparable Nordic systems.

A simulation-based sensitivity analysis quantifying model uncertainty. A 44-run OAT sensitivity analysis across eight parameters identifies η and electricity cost (λ_{high}) as the two most consequential uncertain parameters, while TES sizing shows limited influence at the Vaskiluoto scale. This analysis distinguishes robust qualitative conclusions from quantitative estimates that carry real-world uncertainty, providing a transparent basis for interpreting the results in a planning and investment context.

5.3 Practical Implications

The findings carry direct practical implications for DH operators. DC-P P-D is the recommended configuration for new HP investments, WW T-D for supply security, P-D dispatch as a flexible operational mode with annually recalibrated price thresholds alongside auxiliary backup capacity. TES energy capacity and charge/discharge power rate should be considered separately rather than as a single sizing parameter. For continuously operating sources E_{max}produces slightly larger DCR effects than P_{max}, favouring larger storage volumes. For intermittent industrial sources, the relationship reverses. The charge rate becomes the more relevant constraint as the HP captures heat in short bursts during industrial load peaks. Future TES investment decisions at the Vaskiluoto scale should therefore consider both dimensions rather than defaulting to maximising energy capacity alone.

5.4 Future Work

The methodological boundaries of this study are defined in section 1.4.2, and several directions for future work emerge from these limitations.

The most immediate extension concerns the network representation. The single thermal node DH system modelled in this study is sufficient for energy balance and control strategy analysis but does not capture pipe heat losses, transmission delays, or pressure dynamics. A multi-node network hydraulic model (using tools such as STANET or OpenModelica) would allow these effects to be quantified and would give a more realistic picture

of how supply temperatures and demand coverage change along the distribution network under different HP operating modes.

A second direction concerns the control strategy. The TD and P-D strategies evaluated here are rule-based and practically implementable, but do not exploit the full optimization potential of model predictive control. Future work should benchmark these strategies against MPC using day-ahead price and demand forecasts to quantify the performance gap and the value of forecast accuracy under Finnish market conditions.

The HP performance model is another area worth improving. The static Carnot model with $\eta = 0.50$ introduces ±20% SPF uncertainty as the sensitivity analysis shows. Incorporating manufacturer performance maps that account for partial-load operation, defrost cycling, and start-stop losses would reduce this uncertainty considerably.

Finally, while this thesis focuses on technical and environmental performance, investment decisions ultimately require economic justification. Extending the work to include capital costs, levelized cost of heat across the source configurations, and a full life cycle assessment covering embodied carbon and refrigerant effects would complete the picture and make the findings directly usable for Vaasa DH investment planning.

References

Arnaudo, M., Dalgren, J., Topel, M., & Laumert, B. (2021). Waste heat recovery in low temperature networks versus domestic heat pumps - A techno-economic and environmental analysis. *Energy*, *219*. https://doi.org/10.1016/j.energy.2020.119675

Averfalk, H., & Werner, S. (2017). Essential improvements in future district heating systems. *Energy Procedia*, *116*, 217–225. https://doi.org/10.1016/j.egypro.2017.05.069

Barco-Burgos, J., Bruno, J. C., Eicker, U., Saldaña-Robles, A. L., & Alcántar-Camarena, V. (2022). Review on the integration of high-temperature heat pumps in district heating and cooling networks. *Energy*, *239*. https://doi.org/10.1016/j.energy.2021.122378

Capone, M., Guelpa, E., & Verda, V. (2023). Optimal Installation of Heat Pumps in Large District Heating Networks. *Energies*, *16*(3). https://doi.org/10.3390/en16031448

Christensen, T. B. K., Lund, H., & Sorknæs, P. (2024). The role of thermal energy storages in future smart energy systems. *Energy*, *313*(November), 133948. https://doi.org/10.1016/j.energy.2024.133948

Cioccolanti, L., Renzi, M., Comodi, G., & Rossi, M. (2021). District heating potential in the case of low-grade waste heat recovery from energy intensive industries. *Applied Thermal Engineering*, *191*. https://doi.org/10.1016/j.applthermaleng.2021.116851

Cloutman-Green, E., Barbosa, V. L., Jimenez, D., Wong, D., Dunn, H., Needham, B., Ciric, L., & Hartley, J. C. (2019). Controlling Legionella pneumophila in water systems at reduced hot water temperatures with copper and silver ionization. *American Journal of Infection Control*, *47*(7), 761–766. https://doi.org/10.1016/j.ajic.2018.12.005

Cudok, F., Giannetti, N., Ciganda, J. L. C., Aoyama, J., Babu, P., Coronas, A., Fujii, T., Inoue, N., Saito, K., Yamaguchi, S., & Ziegler, F. (2021). Absorption heat transformer - state-of-the-art of industrial applications. *Renewable and Sustainable Energy Reviews*, *141*(January). https://doi.org/10.1016/j.rser.2021.110757

Dancker, J., & Wolter, M. (2021). Improved quasi-steady-state power flow calculation for district heating systems: A coupled Newton-Raphson approach. *Applied Energy*, *295*(December 2020), 116930. https://doi.org/10.1016/j.apenergy.2021.116930

Danielewicz, J., Śniechowska, B., Sayegh, M. A., Fidorów, N., & Jouhara, H. (2016). Three-dimensional numerical model of heat losses from district heating network pre-insulated pipes buried in the ground. *Energy*, *108*, 172–184. https://doi.org/10.1016/j.energy.2015.07.012

David, A., Mathiesen, B. V., Averfalk, H., Werner, S., & Lund, H. (2017). Heat Roadmap Europe: Large-scale electric heat pumps in district heating systems. In *Energies* (Vol. 10, Number 4). MDPI AG. https://doi.org/10.3390/en10040578

Dibos, S., Pesch, T., & Benigni, A. (2024). HeatNetSim: An open-source simulation tool for heating and cooling networks suitable for future energy systems. *Energy*, *312*(December 2023). https://doi.org/10.1016/j.energy.2024.133588

Drgoňa, J., Arroyo, J., Cupeiro Figueroa, I., Blum, D., Arendt, K., Kim, D., Ollé, E. P., Oravec, J., Wetter, M., Vrabie, D. L., & Helsen, L. (2020). All you need to know about model predictive control for buildings. *Annual Reviews in Control*, *50*(May), 190–232. https://doi.org/10.1016/j.arcontrol.2020.09.001

Elomatic. (2024). *ELOMATIC*. https://www.elomatic.com/news/future-heat-plant-in-pattis-vaasa-converts-waste-water-heat-into-district-heating/

Energiateollisuus ry. (2025). *Finnish Energy*. https://energia.fi/wp-content/uploads/2025/01/Electricity-Year-2024_20250115.pdf

Euroheat & Power. (2022). *LARGE HEAT PUMPS IN DISTRICT HEATING & COOLING SYSTEMS*. https://build-up.ec.europa.eu/sites/default/files/content/v18-technology-report-large-heat-pumps-in-district-heating-and-cooling-systems.pdf

Euroheat & Power. (2025). *Towards a sustainable, resilient and competitive heating sector by 2050.* https://api.euroheat.org/uploads/Euroheat_and_Power_Executive_summary_2050_study_f5fe43e503.pdf

European Commission - JRC. (2025). *Heat Pumps in the European Union Status Report on Technology Development, Trends, Value Chains and Markets*. https://doi.org/10.2760/6476347

Fang, H., Xia, J., Zhu, K., Su, Y., & Jiang, Y. (2013). Industrial waste heat utilization for low temperature district heating. *Energy Policy*, *62*, 236–246. https://doi.org/10.1016/j.enpol.2013.06.104

Fingrid. (2026). *FINGRID*. https://data.fingrid.fi/en/datasets/265

Finnish Energy. (2026). *Finnish Energy*. https://energia.fi/en/statistics/statistics-on-district-heating/

FMI. (2026). *Finnish Meteorological Institute*. https://en.ilmatieteenlaitos.fi/download-observations#!/

Friedrich, P., Kuroptev, K., Huynh, T., & Niessen, S. (2025). Stability Analysis and Mitigation of Thermo-Hydraulic Oscillations in Multi-Supplier District Heating Systems. *Energies*, *18*(5). https://doi.org/10.3390/en18051126

Gasser, L., Flück, S., Kleingries, M., Meier, C., & Bätschmann, M. (2017). *High efficiency heat pumps for low temperature lift applications. In 12th IEA heat pump conference. Rotterdam.*

Gjorgievski, V. Z., Markovska, N., Abazi, A., & Duić, N. (2021). The potential of power-to-heat demand response to improve the flexibility of the energy system: An empirical review. *Renewable and Sustainable Energy Reviews*, *138*(December 2019). https://doi.org/10.1016/j.rser.2020.110489

Gómez- de- Arteche -Botas, M., Iturralde- Iñarga, J., & Fúnez-Guerra, C. (2025). Heat pump integration for waste heat recovery from a 20 MWe green hydrogen plant to increase global efficiency. *International Journal of Hydrogen Energy*, *142*(April), 777–783. https://doi.org/10.1016/j.ijhydene.2025.04.202

Gong, Y., Liu, F., Sui, J., Lv, Y., & Wang, Y. (2025). Thermodynamic investigation of ternary ionic liquid working pairs and application in absorption heat transformers. *International Journal of Refrigeration*, *179*(July), 107–120. https://doi.org/10.1016/j.ijrefrig.2025.07.027

Guelpa, E., & Verda, V. (2019). Thermal energy storage in district heating and cooling systems: A review. *Applied Energy*, *252*(June), 113474. https://doi.org/10.1016/j.apenergy.2019.113474

Han, Z., Xue, D., Wei, H., Ji, Q., Sun, X., & Li, X. (2021). Study on operation strategy of evaporative cooling composite air conditioning system in data center. *Renewable Energy*, *177*, 1147–1160. https://doi.org/10.1016/j.renene.2021.06.046

IEA DHC. (2024). *INTERNATIONAL ENERGY AGENCY TECHNOLOGY COLLABORATION PROGRAMME ON DISTRICT HEATING AND COOLING*. www.iea-dhc.org.

Ivezić, D. D., Živković, M. A., Manić, D. J., Madžarević, A. R., Pavlović, B. S., & Danilović, D. (2023). EVALUATION OF THE EFFECTS OF WASTEWATER HEAT PUMP INTEGRATION INTO DISTRICT HEATING SYSTEMS BY SIMULATION. *Thermal Science*, *27*(3), 2443–2454. https://doi.org/10.2298/TSCI220813168I

Jaanto, J., Sihvonen, V., Honkapuro, S., Riikonen, J., Price, A., Ylönen, M., & Kivioja, V. (2023). Thermal storage deployment in the framework of current electricity market design. *International Conference on the European Energy Market, EEM*, *2023-June*. https://doi.org/10.1109/EEM58374.2023.10161744

Javanshir, N., Syri, S., Teräsvirta, A., & Olkkonen, V. (2022). Abandoning peat in a city district heat system with wind power, heat pumps, and heat storage. *Energy Reports*, *8*(2022), 3051–3062. https://doi.org/10.1016/j.egyr.2022.02.064

Ji, Q., Li, Y., Yin, Y., Che, C., & Huang, G. (2026). Compression-absorption hybrid heat pumps operating wide temperature ranges: A review and perspectives for large temperature lift. *Applied Energy*, *405*(December 2025), 127217. https://doi.org/10.1016/j.apenergy.2025.127217

Jiang, J., Hu, B., Wang, R. Z., Deng, N., Cao, F., & Wang, C. C. (2022). A review and perspective on industry high-temperature heat pumps. *Renewable and Sustainable Energy Reviews*, *161*(January), 112106. https://doi.org/10.1016/j.rser.2022.112106

Jodeiri, A. M., Goldsworthy, M. J., Buffa, S., & Cozzini, M. (2022). Role of sustainable heat sources in transition towards fourth generation district heating – A review. *Renewable and Sustainable Energy Reviews*, *158*(January 2022), 112156. https://doi.org/10.1016/j.rser.2022.112156

Jokinen, I., Lund, A., Hirvonen, J., Jokisalo, J., Kosonen, R., & Lehtonen, M. (2022). Coupling of the electricity and district heat generation sectors with building stock energy retrofits as a measure to reduce carbon emissions. *Energy Conversion and*

Management, *269*(July), 115961. https://doi.org/10.1016/j.enconman.2022.115961

Jouhara, H., Khordehgah, N., Almahmoud, S., Delpech, B., Chauhan, A., & Tassou, S. A. (2018). Waste heat recovery technologies and applications. *Thermal Science and Engineering Progress*, *6*(April), 268–289. https://doi.org/10.1016/j.tsep.2018.04.017

Kuntuarova, S., Lickleder, T., Huynh, T., Zinsmeister, D., Hamacher, T., & Perić, V. (2024). Design and simulation of district heating networks: A review of modeling approaches and tools. *Energy*, *305*. https://doi.org/10.1016/j.energy.2024.132189

Kuta, M., Mlonka-Mędrala, A., Radomska, E., & Gołdasz, A. (2025). Mobile Thermal Energy Storage—A Review and Analysis in the Context of Waste Heat Recovery. In *Energies* (Vol. 18, Number 15). Multidisciplinary Digital Publishing Institute (MDPI). https://doi.org/10.3390/en18154136

Lavikainen, V., & Fränti, P. (2024). Clustering district heating customers based on load profiles. *Applied Computing and Intelligence*, *4*(2), 269–281. https://doi.org/10.3934/aci.2024016

Lieskoski, S., Koskinen, O., Tuuf, J., & Björklund-Sänkiaho, M. (2024). A review of the current status of energy storage in Finland and future development prospects. In *Journal of Energy Storage* (Vol. 93). Elsevier Ltd. https://doi.org/10.1016/j.est.2024.112327

Lorenzo, C., & Narvarte, L. (2019). Performance indicators of photovoltaic heat-pumps. *Heliyon*, *5*(10), e02691. https://doi.org/10.1016/j.heliyon.2019.e02691

Lu, T., Lü, X., Välisuo, P., Zhang, Q., & Clements-Croome, D. (2024). Innovative approaches for deep decarbonization of data centers and building space heating networks: Modeling and comparison of novel waste heat recovery systems for liquid cooling systems. *Applied Energy*, *357*(August 2023). https://doi.org/10.1016/j.apenergy.2023.122473

Lund, H. (2018). Renewable heating strategies and their consequences for storage and grid infrastructures comparing a smart grid to a smart energy systems approach. *Energy*, *151*, 94–102. https://doi.org/10.1016/j.energy.2018.03.010

Lund, H., Werner, S., Wiltshire, R., Svendsen, S., Thorsen, J. E., Hvelplund, F., & Mathiesen, B. V. (2014). 4th Generation District Heating (4GDH). Integrating smart thermal grids into future sustainable energy systems. *Energy*, *68*, 1–11. https://doi.org/10.1016/j.energy.2014.02.089

Ma, X., Du, Y., Zhao, T., Zhu, T., Lei, B., & Wu, Y. (2024). A comprehensive review of compression high-temperature heat pump steam system: Status and trend. *International Journal of Refrigeration*, *164*(100), 218–242. https://doi.org/10.1016/j.ijrefrig.2024.04.024

Mahmoud, M., Ramadan, M., Naher, S., Pullen, K., Baroutaji, A., & Olabi, A. G. (2020). Recent advances in district energy systems: A review. *Thermal Science and Engineering Progress*, *20*(August), 100678. https://doi.org/10.1016/j.tsep.2020.100678

MathWorks. (2026). *MathWorks*. https://se.mathworks.com/solutions/system-modeling-simulation.html

Meibodi, S. S., & Loveridge, F. (2022). The future role of energy geostructures in fifth generation district heating and cooling networks. *Energy*, *240*, 122481. https://doi.org/10.1016/j.energy.2021.122481

Mugnini, A., Evens, M., & Arteconi, A. (2024). Model predictive controls for residential buildings with heat pumps: Experimentally validated archetypes to simplify the large-scale application. *Energy and Buildings*, *320*(August), 114632. https://doi.org/10.1016/j.enbuild.2024.114632

Nérot, B., Lamaison, N., Mabrouk, M. T., Bavière, R., & Lacarrière, B. (2023). Optimization framework for evaluating urban thermal systems potential. *Energy*, *270*(February). https://doi.org/10.1016/j.energy.2023.126851

Nord, N., Løve Nielsen, E. K., Kauko, H., & Tereshchenko, T. (2018). Challenges and potentials for low-temperature district heating implementation in Norway. *Energy*, *151*, 889–902. https://doi.org/10.1016/j.energy.2018.03.094

Ochs, F., Magni, M., & Dermentzis, G. (2022). Integration of Heat Pumps in Buildings and District Heating Systems—Evaluation on a Building and Energy System Level. *Energies*, *15*(11). https://doi.org/10.3390/en15113889

Opadokun, O., Tao, Y. X., & Lamb, J. (2025). A review of waste heat sources for district heating. *Energy Reports*, *14*(April), 1051–1070. https://doi.org/10.1016/j.egyr.2025.07.015

Østergaard, D. S., Smith, K. M., Tunzi, M., & Svendsen, S. (2022). Low-temperature operation of heating systems to enable 4th generation district heating: A review. *Energy*, *248*. https://doi.org/10.1016/j.energy.2022.123529

Østergaard, D., & Svendsen, S. (2017). Space heating with ultra-low-temperature district heating - A case study of four single-family houses from the 1980s. *Energy Procedia*, *116*, 226–235. https://doi.org/10.1016/j.egypro.2017.05.070

Oulun Energia. (2023). *Oulun Energia*. https://www.oulunenergia.fi/en/whats-new/blog/district-heating-costs-in-single-family-houses-from-initial-investment-to-the-end-of-its-life-cycle/

Pakere, I., Blumberga, D., Volkova, A., Lepiksaar, K., & Zirne, A. (2023). Valorisation of Waste Heat in Existing and Future District Heating Systems. *Energies*, *16*(19). https://doi.org/10.3390/en16196796

Pan, Q., Peng, J., & Wang, R. (2021). Application analysis of adsorption refrigeration system for solar and data center waste heat utilization. *Energy Conversion and Management*, *228*, 113564. https://doi.org/10.1016/j.enconman.2020.113564

Pastore, L. M. (2026). Sector Coupling and Flexibility Measures in Distributed Renewable Energy Systems: A Comprehensive Review. *Sustainability (Switzerland)*, *18*(1). https://doi.org/10.3390/su18010437

Péan, T. Q., Salom, J., & Costa-Castelló, R. (2019). Review of control strategies for improving the energy flexibility provided by heat pump systems in buildings. *Journal of Process Control*, *74*, 35–49. https://doi.org/10.1016/j.jprocont.2018.03.006

Pieper, H., Mašatin, V., Volkova, A., Ommen, T., Elmegaard, B., & Markussen, W. B. (2019). Modelling framework for integration of large-scale heat pumps in district heating using low-temperature heat sources: A case study of Tallinn, Estonia. *International Journal of Sustainable Energy Planning and Management*, *20*, 67–86. https://doi.org/10.5278/ijsepm.2019.20.6

Pipiciello, M., Trentin, F., Soppelsa, A., Menegon, D., Fedrizzi, R., Ricci, M., Di Pietra, B., & Sdringola, P. (2024). The bidirectional substation for district heating users: experimental performance assessment with operational profiles of prosumer loads and distributed generation. *Energy and Buildings*, *305*. https://doi.org/10.1016/j.enbuild.2023.113872

ROKA3. (2026). *ROKA3*. https://roka3.com/

Sandhaas, A., Kim, H., De Jesús, C., & Hartmann, N. (2022). *Generation of Industrial Electricity and Heat Demand Profiles for Energy System Analysis*. 1–14.

Schmidt, D., Kallert, A., Blesl, M., Svendsen, S., Li, H., Nord, N., & Sipilä, K. (2017). Low Temperature District Heating for Future Energy Systems. *Energy Procedia*, *116*, 26–38. https://doi.org/10.1016/j.egypro.2017.05.052

STANET. (2026). *STANET - Network analysis for gas, water, electricity, district heating and sewage*. https://www.stafu.de/en/product.html

Stanica, D. I., Bachmann, M., & Kriegel, M. (2021). Design and performance of a multi-level cascading district heating network with multiple prosumers and energy storage. *Energy Reports*, *7*, 128–139. https://doi.org/10.1016/j.egyr.2021.08.163

Tan, Y., An, L., Wang, L., Hou, Z., Zhao, S., Liu, B., & Guo, Y. (2024). Proposal and performance evaluation of a solar hybrid heat pump with integrated air-source compression cycle. *Energy Conversion and Management*, *321*(September), 119097. https://doi.org/10.1016/j.enconman.2024.119097

Tejani, A. (2021). Assessing the Efficiency of Heat Pumps in Cold Climates: A Study Focused on Performance Metrics. *ESP Journal of Engineering & Technology Advancements*, *1*(1), 47–56. https://doi.org/10.56472/25832646/JETA-V1I1P108

Toffanin, R., Curti, V., & Barbato, M. C. (2021). Impact of Legionella regulation on a 4th generation district heating substation energy use and cost: the case of a Swiss single-family household. *Energy*, *228*. https://doi.org/10.1016/j.energy.2021.120473

Transparency Platform. (2026). *Transparency platform: Electricity generation, transportation and consumption for the European mark*. https://transparency.entsoe.eu/market/energyPrices

TRNSYS. (2026). *TRNSYS: Transsolar softwareengineering*. https://trnsys.de/

Turek, V., Kilkovský, B., Daxner, J., Babička Fialová, D., & Jegla, Z. (2024). Industrial Waste Heat Utilization in the European Union—An Engineering-Centric Review. *Energies*, *17*(9). https://doi.org/10.3390/en17092084

Vaasan Sähkö. (2025). *Vaasan Sähkö*. https://www.vaasansahko.fi/en/district-heating/district-heating-production/

Vaasan Sähkö. (2026). *VAASAN SÄHKÖ*. https://www.vaasansahko.fi/en/district-heating/origin-of-heat-2024/

Vaasan Vesi. (2024). *VAASAN VESI: VASA VATTEN*. https://www.vaasanvesi.fi/pattin-puhdistamo

Vaasan Voima. (2023). *Vaasan Voima*. https://www.vaasanvoima.fi/en/finlands-largest-electric-boiler-and-thermal-energy-storage-combination-launched-in-vaasa/

Vaasan Voima. (2024). *Vaasan Voima*. https://www.vaasanvoima.fi/en/vaasan-voima-to-grow-the-capacity-of-its-thermal-energy-storage-facility/

Vaissalo, J., Dutta, A., Bouri, E., & Azoury, N. (2024). Carbon emission allowances and Nordic electricity markets: Linkages and hedging analysis. *Energy Reports*, *12*(September), 2845–2854. https://doi.org/10.1016/j.egyr.2024.08.072

Vannoni, A., Sorce, A., Traverso, A., & Fausto Massardo, A. (2023). Large size heat pumps advanced cost functions introducing the impact of design COP on capital costs. *Energy*, *284*(July), 129204. https://doi.org/10.1016/j.energy.2023.129204

Wahlroos, M., Pärssinen, M., Manner, J., & Syri, S. (2017). Utilizing data center waste heat in district heating – Impacts on energy efficiency and prospects for low-temperature district heating networks. *Energy*, *140*(2017), 1228–1238. https://doi.org/10.1016/j.energy.2017.08.078

Wang, Y., Zhang, R., Meriläinen, A., Kosonen, A., Jokisalo, J., & Kosonen, R. (2025). Cost-optimal control for a small energy community heated with dual source heat pump and district heating. *Energy and Buildings*, *336*(January). https://doi.org/10.1016/j.enbuild.2025.115622

Werner, S. (2017). International review of district heating and cooling. *Energy*, *137*, 617–631. https://doi.org/10.1016/j.energy.2017.04.045

Winterscheid, C., Holler, S., & Dalenbäck, J. O. (2017). Integration of solar thermal systems into existing district heating systems. *Energy Procedia*, *116*, 158–169. https://doi.org/10.1016/j.egypro.2017.05.064

WSTAR. (2025). *VAMK*. https://www.vamk.fi/en/ajankohtaista/a-new-zero-emission-research-environment-completed-in-vaasa-wstar-offers-solutions-for-data-center-energy-efficiency

Wu, D., Hu, B., & Wang, R. Z. (2021). Vapor compression heat pumps with pure Low-GWP refrigerants. *Renewable and Sustainable Energy Reviews*, *138*(April 2020). https://doi.org/10.1016/j.rser.2020.110571

Xu, J., Wang, R. Z., & Li, Y. (2014). A review of available technologies for seasonal thermal energy storage. *Solar Energy*, *103*, 610–638. https://doi.org/10.1016/j.solener.2013.06.006

Xu, Z. Y., Wang, R. Z., & Yang, C. (2019). Perspectives for low-temperature waste heat recovery. *Energy*, *176*, 1037–1043. https://doi.org/10.1016/j.energy.2019.04.001

Yuan, X., Liang, Y., Hu, X., Xu, Y., Chen, Y., & Kosonen, R. (2023). Waste heat recoveries in data centers: A review. *Renewable and Sustainable Energy Reviews*, *188*(October), 113777. https://doi.org/10.1016/j.rser.2023.113777

Yuan, X., Liu, J., Sun, S., Lin, X., Fan, X., Zhao, W., & Kosonen, R. (2025). Data center waste heat for district heating networks: A review. *Renewable and Sustainable Energy Reviews*, *219*(May), 115863. https://doi.org/10.1016/j.rser.2025.115863

Zhai, C., & Wu, W. (2021). Heat and mass transfer performance comparison of various absorbers/desorbers towards compact and efficient absorption heat pumps. *International Journal of Refrigeration*, *127*, 203–220. https://doi.org/10.1016/j.ijrefrig.2021.01.029

Zhang, S., Gu, W., Lu, S., Yao, S., Zhou, S., & Chen, X. (2021). Dynamic Security Control in Heat and Electricity Integrated Energy System with an Equivalent Heating Network Model. *IEEE Transactions on Smart Grid*, *12*(6), 4788–4798. https://doi.org/10.1109/TSG.2021.3102057

Zirne, M. A., & Pakere, I. (2024). Integrating Low-temperature Waste Heat in District Heating Systems. Legal Framework and Pricing. *Environmental and Climate Technologies*, *28*(1). https://doi.org/10.2478/rtuect-2024-0067

Appendices

Appendix A. Input Data and Boundary Conditions

I. Annual District Heating Demand Profile and Seasonal Pattern

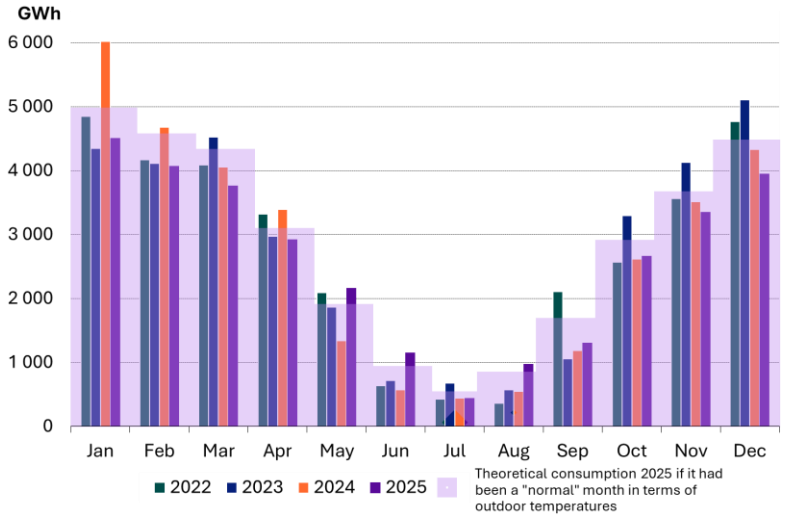

Figure A 1: Typical Finnish monthly DH demand pattern (Finnish Energy, 2026).

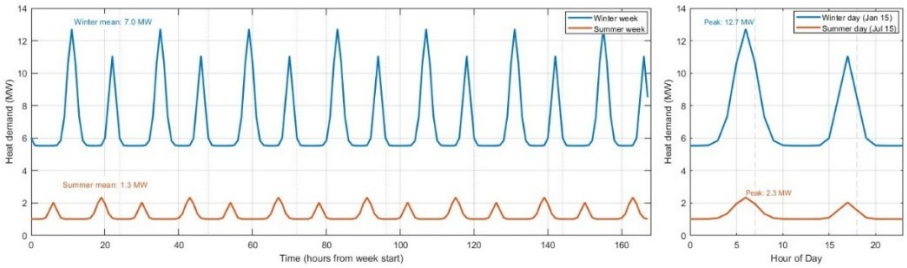

Figure A 2: Modelled typical week: Winter vs summer demand patterns(left) and daily demand pattern (right).

II. Finnish Day-Ahead Electricity Prices, 2024

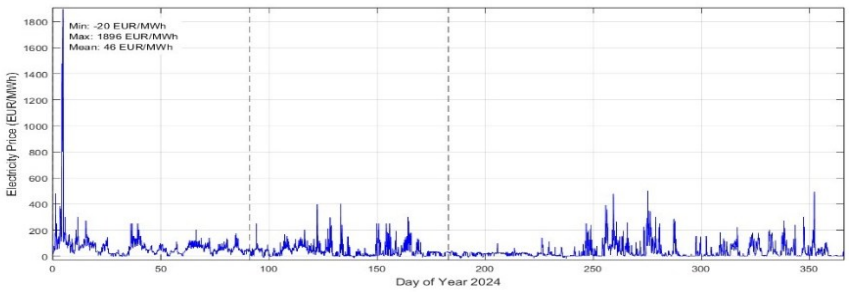

Figure A 3: 2024 Day-Ahead Electricity Prices in Finland (Transparency Platform, 2026).

III. Ambient Air Temperature, Vaasa, 2024

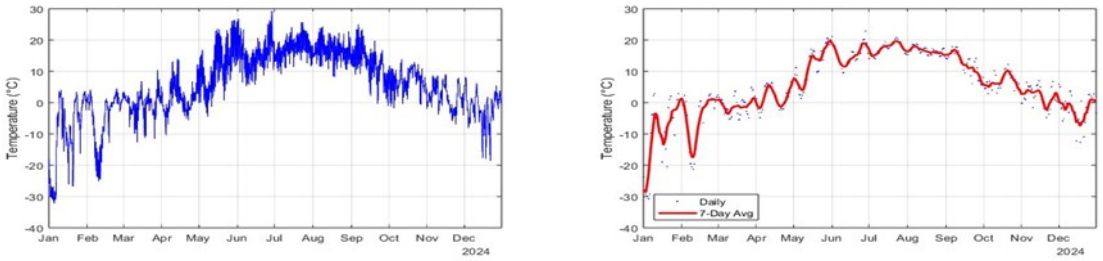

Figure A 4: Hourly Temperature (left) and Daily Average with 7-Day Trend(right).

IV. Grid CO_2 Emission Factor, Finland, 2024

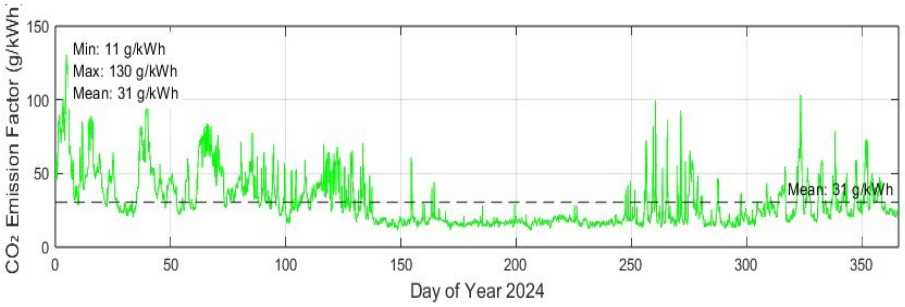

Figure A 5: Real-Time annual CO_2 Emission Factor for Electricity Consumption in Finland.

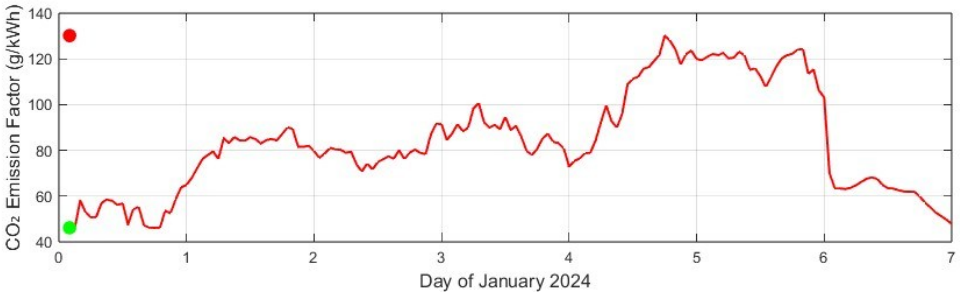

Figure A 6: First Week of January 2024 - Hourly CO_2 Emission Factor.

Appendix 2. Waste Heat Source Characterization

i. Pått WW Source Heat and Temperature Profile

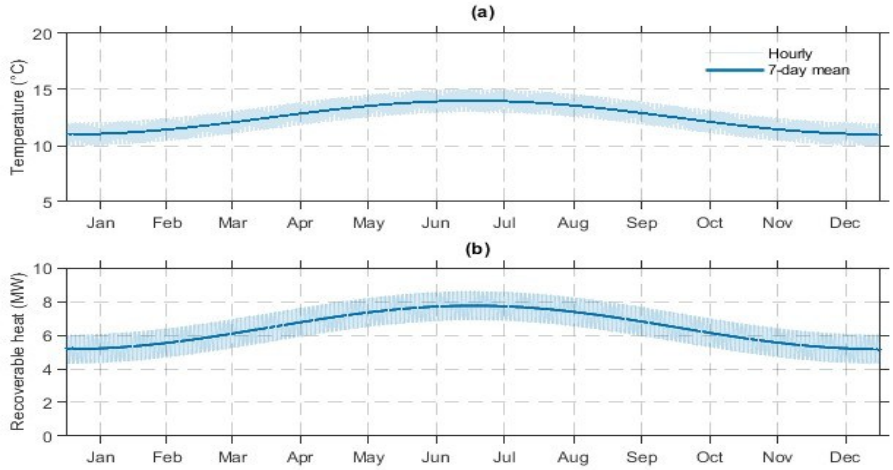

Figure B 1: Hourly source temperature (grey) and 7-day rolling mean (blue) for the Pått WW source: (a) source temperature, seasonal range 10-15°C; (b) recoverable heat capacity, mean 6.46MW.

ii. Data Center Waste Heat Source Profiles

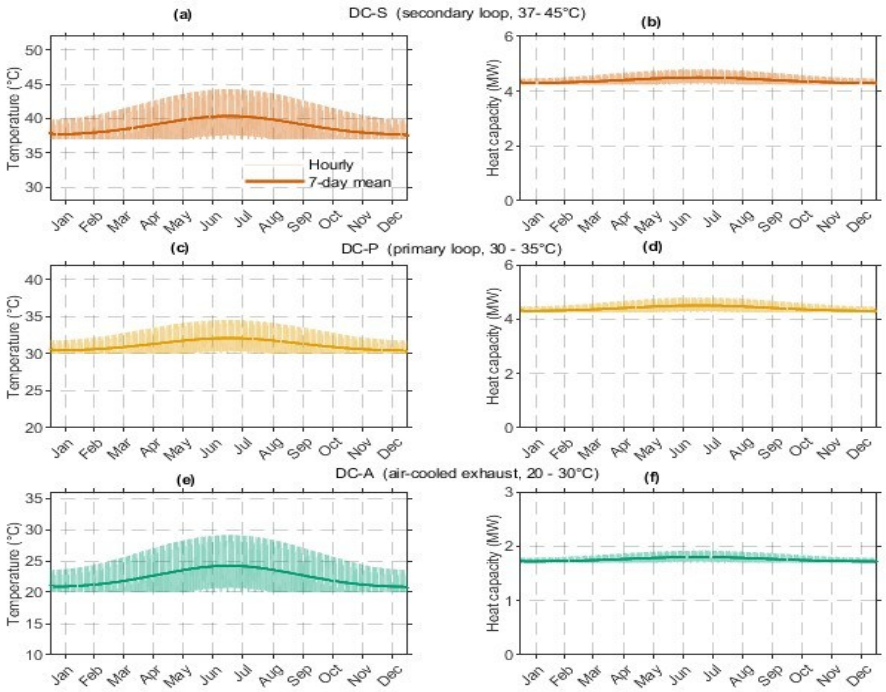

Figure B 2: Data center waste heat source profiles for all three modelled configurations: (a, c, e) hourly and 7-day mean source temperature; (b, d, f) available heat capacity for DC-S, DC-P, and DC-A, respectively.

iii. IWH Source Profiles - January Dynamics

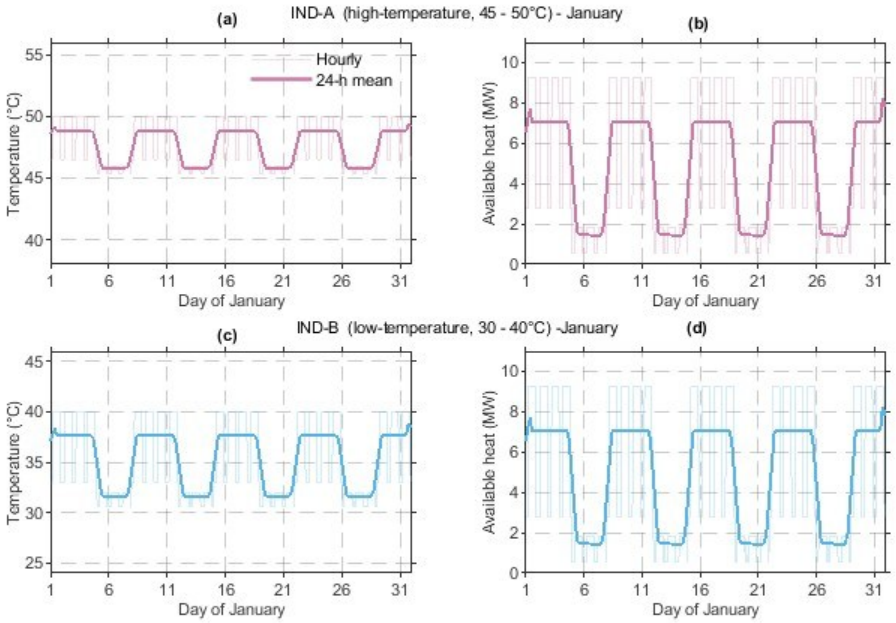

Figure B 3: IWH source dynamics for January 2024: (a, c) hourly and 24-hour mean source temperature; (b, d) available heat capacity for IND-A and IND-B.

iv. All-Source Temperature Comparison and Distribution

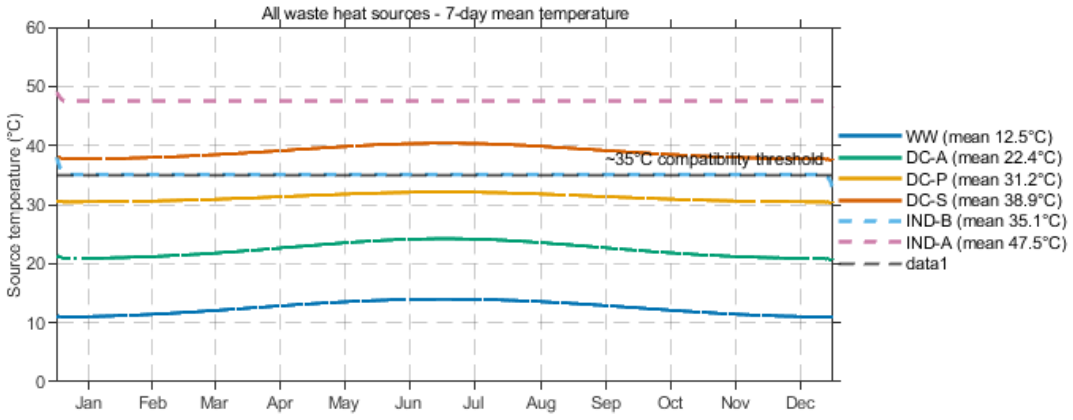

Figure B 4: Seven-day mean source temperatures for all six waste heat configurations throughout 2024. The dashed line at 35°C marks the approximate HP-LTDH compatibility threshold above which warm-season blocking occurs.